Article

Current Biology

Theta Rhythmic Neuronal Activity and Reaction Times Arising from Cortical Receptive Field Interactions during Distributed Attention

Highlights

- Receptive field interactions induce theta rhythmic activation in visual cortex
- The neuronal rhythm does not depend on small fixational eye movements
- Reaction time fluctuations lock to the neuronal rhythm under distributed attention

Authors

Ricardo Kienitz, Joscha T. Schmiedt, Katharine A. Shapcott, Kleopatra Kouroupaki, Richard C. Saunders, Michael Christoph Schmid

Correspondence

michael.schmid@ncl.ac.uk

In Brief

Kienitz et al. show that receptive field interactions induce theta rhythmic neuronal activity in visual area V4 that is independent of eye movements. Under distributed attention, periodic reaction times were locked to the neuronal rhythm. Rhythmic modulation of neuronal sensitivity could thus explain attentional dynamics during visual competition.

Kienitz et al., 2018, Current Biology *28*, 2377–2387
August 6, 2018
https://doi.org/10.1016/j.cub.2018.05.086

CellPress

Current Biology
Article

Theta Rhythmic Neuronal Activity and Reaction Times Arising from Cortical Receptive Field Interactions during Distributed Attention

Ricardo Kienitz,[1,2,4] Joscha T. Schmiedt,[1] Katharine A. Shapcott,[1] Kleopatra Kouroupaki,[1] Richard C. Saunders,[3] and Michael Christoph Schmid[1,4,5,*]
[1]Ernst Strüngmann Institute (ESI) for Neuroscience in Cooperation with the Max Planck Society, Deutschordenstraße 46, 60528 Frankfurt a.M., Germany
[2]Epilepsy Center Frankfurt Rhine-Main, Center of Neurology and Neurosurgery, Goethe University, Schleusenweg 2-16, 60528 Frankfurt a.M., Germany
[3]Laboratory of Neuropsychology, NIMH, 49 Convent Drive, Bethesda, MD 20892, USA
[4]Institute of Neuroscience, Newcastle University, Framlington Place, Newcastle upon Tyne NE2 4HH, UK
[5]Lead Contact
*Correspondence: michael.schmid@ncl.ac.uk
https://doi.org/10.1016/j.cub.2018.05.086

SUMMARY

Growing evidence suggests that distributed spatial attention may invoke theta (3–9 Hz) rhythmic sampling processes. The neuronal basis of such attentional sampling is, however, not fully understood. Here we show using array recordings in visual cortical area V4 of two awake macaques that presenting separate visual stimuli to the excitatory center and suppressive surround of neuronal receptive fields (RFs) elicits rhythmic multi-unit activity (MUA) at 3–6 Hz. This neuronal rhythm did not depend on small fixational eye movements. In the context of a distributed spatial attention task, during which the monkeys detected a spatially and temporally uncertain target, reaction times (RTs) exhibited similar rhythmic fluctuations. RTs were fast or slow depending on the target occurrence during high or low MUA, resulting in rhythmic MUA-RT cross-correlations at theta frequencies. These findings show that theta rhythmic neuronal activity can arise from competitive RF interactions and that this rhythm may result in rhythmic RTs potentially subserving attentional sampling.

INTRODUCTION

Spatial attention can exhibit fluctuations that under some tested conditions might be rhythmic. In vision, this is apparent, for example, during overt saccadic exploration of visual scenes, during which periods of fixation tend to occur every ~200 ms, i.e., in the slow theta range [1, 2]. Similar rhythmic exploration is sometimes also observed during apparent fixation periods when subjects perform fast fixational eye movements (microsaccades; MSs) [1, 3]. Such rhythmic sampling phenomena appear to not be limited to overt behavior but have also been discovered in investigations of covert distributed spatial attention, i.e., in the absence of overt eye movements. Here the subject's capacity to detect a change in one of multiple objects is assessed as a function of trial-by-trial varying target onset times. A convergent finding across several recent studies is a theta (3–9 Hz) rhythmic sampling that can be observed in performance or reaction time (RT) measures during such distributed attention conditions [4–6]. For example, in a study by Fiebelkorn et al. [7], subjects had to detect a target on one of three possible target positions whereby two positions belonged to the same underlying object and one position belonged to an alternative object. The results confirmed a theta rhythmic modulation of detection performance under these task conditions. The phase of the rhythm depended on the target location, such that faster RTs to one location alternated with those to the alternative location of the same object. It therefore appears that the brain might engage a spatial sampling mechanism that operates in the theta range when two or more objects are simultaneously monitored.

Electroencephalography (EEG) and magnetoencephalography (MEG) studies in humans have confirmed the presence of rhythmic oscillatory responses during a variety of attention tasks [5, 8–12]. For example, theta oscillations were measured over visual cortex during tasks that required the tracking of multiple objects, where theta appeared to influence the detectability of a visual target (e.g., [5, 10, 12, 13]). Reports from intracranial neuronal recordings in fixating monkeys sometimes contain theta rhythmic activation in V4 and inferotemporal cortex (IT) [14–17], but the mechanism generating this rhythm and its possible relationship to attentional sampling remain unclear. Two recent studies linked theta and gamma oscillations to MS occurrences [18, 19]. However, it is unclear whether MSs constitute a prerequisite for the neuronal rhythm to emerge or whether it can also occur independently, in which case the neuronal mechanism generating the rhythm still remains unknown. To address this, we recorded multi-unit activity (MUA) from V4 neurons while monkeys performed a task invoking attentional sampling. We focused on area V4 because neuronal activity of this area is known to be well associated with attention: lesions of V4 result in an attentional stimulus selection deficit [20]. The firing of many V4 neurons is modulated by MSs [19, 21, 22]

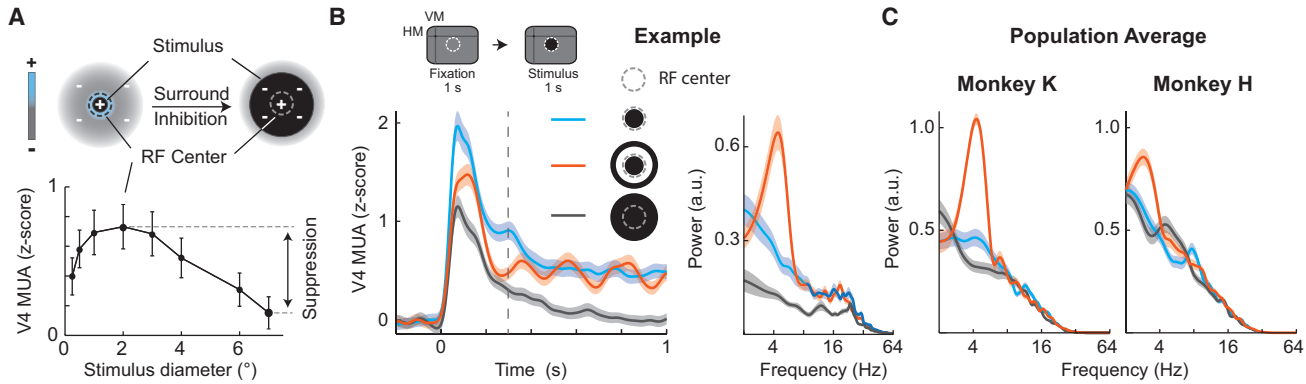

Figure 1. Theta Modulation of MUA Arises from RF Center-Surround Interactions

(A) Receptive field (RF) composition with an excitatory center (blue) and a suppressive surround (gray). Small and large stimuli (black disks) are shown to illustrate their relationship with RF structures. Lower: example size tuning curve from one representative MUA channel from monkey K (suppression index [SI] 0.78, based on ~100 trials per condition).

(B) Upper: passive viewing task; the dotted circles indicate the excitatory MUA RF center. Left: example MUA response from the same recording electrode as in (A) to three different stimulus configurations: small 2° disk (blue), large 6° disk (gray), and 2° disk with 4°–6° annulus (orange). The vertical dashed line highlights the window for spectral analyses (0.3–1 s). Right: corresponding MUA powerspectra (calculated during 0.3–1 s after stimulus onset). Note the presence of rhythmic activity in the disk-annulus condition only. Shading around lines depicts SEM. VM/HM, vertical/horizontal meridian.

(C) Population powerspectra for the same stimuli as in (B), averaged across channels for monkey K (left; n = 40) and monkey H (right; n = 57). Shading around lines depicts SEM.

See also Figure S1.

and increases when attention is covertly focused on a stimulus in their receptive field (RF) [23, 24]. When in addition to a stimulus in the RF a second stimulus is added to the RF surround, the neuron's response is usually suppressed relative to its response to the center stimulus alone [25, 26]. Focusing attention to the RF center or surround stimulus will enhance or diminish this surround suppression, respectively [24, 27, 28]. We reasoned that during longer stimulus presentation times the spatial structure of V4 neuron RFs into the excitatory center and inhibitory surround might provide the balance of excitation and inhibition that is required for the emergence of oscillatory activity [29, 30], which in turn could constitute the neuronal basis for attentional sampling [13]. To investigate this at the level of neighboring neuronal populations, we implanted "Utah" microelectrode arrays into V4 and measured MUA [31] from the array's 64 electrodes (see STAR Methods). We first investigated how center-surround RF stimulation could evoke theta rhythmic MUA. Because MSs, sometimes occurring every 250–300 ms, have been linked with rhythmic neural responses [18, 19, 32], we also tested their potential contribution to the emergence of theta oscillations. In a final step, we investigated the relationship between theta rhythms in the MUA to the monkeys' RTs during an attentional detection task.

RESULTS

Receptive Field Center and Surround Interactions Induce Theta Rhythmic MUA

To quantify surround suppression in V4 during the passive fixation task, we determined the extent and strength of surround suppression in V4 by systematically increasing the diameter of a disk stimulus presented to a given RF [33]. Stimuli were displayed for 1 s to provide sufficient time to detect oscillatory activity. In all electrodes (40/40 and 57/57 in monkey K and H, respectively; see STAR Methods), increasing disk size resulted in a response increase up to a maximal response at 1°–2° visual degrees (defined as the excitatory RF center; see STAR Methods). Further stimulus size increases led to an average reduction of responses by 62% ± 3% (mean ± SEM; n = 40) and 77% ± 2% (n = 57) in monkey K and H, respectively, i.e., an increase of inhibition or surround suppression (Figures 1A and S1), in line with previous observations [25, 26, 33]. Importantly, no evidence of rhythmic activity was seen under this condition (Figures 1B and 1C).

This situation changed profoundly when the RF center and surround were stimulated separately using spatially separated visual objects (disk-annulus or disk-flanker stimulation; Figures 1B and S2). Only under these stimulus conditions, substantial rhythmic modulation in the theta frequency band (peak frequencies: monkey K, 4.1 ± 0.2 Hz; monkey H, 3.4 ± 0.1 Hz) emerged in the MUA time course as well as its spectral representation in most electrode channels of both monkeys (Figures 1B, 1C, and S1E): 98%, 39/40 electrodes in monkey K; 79%, 45/57 electrodes in monkey H (see STAR Methods). As shown in Figures 1C and S1E, across electrodes the strength of theta power increased on average by 185% ± 27.9% (monkey K) and 158% ± 40.3% (monkey H) in the disk-annulus condition and therefore significantly more compared to the condition when a single large disk with the same outer diameter was presented (−11% ± 7.8% for monkey K and 43% ± 23% for monkey H, $p = 7 \times 10^{-8}$, n = 40 and $p = 2 \times 10^{-5}$, n = 57, respectively, Wilcoxon signed-rank test). Autocorrelograms, another method used to assess rhythmicity, revealed similar results (Figure S1C). Examination of the local-field potential (LFP) revealed also a very similar pattern in that a prominent theta peak was present under disk-annulus stimulation conditions; however, it could also be observed to a

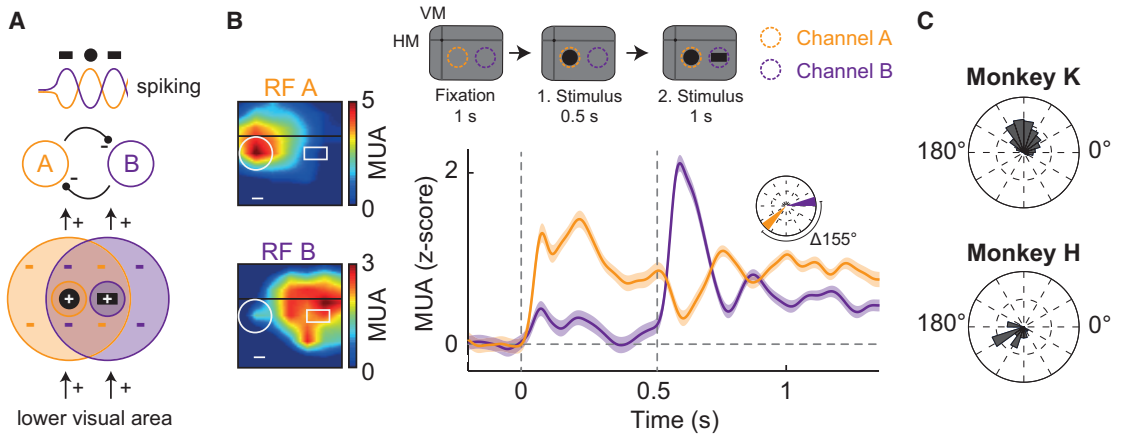

Figure 2. Anti-Phasic Theta Oscillations from Nearby Electrodes with Adjacent RF Coverage

(A) Hypothesized mechanism underlying the neural theta oscillation. If two separate stimuli (e.g., disk and bar, simultaneously presented) each drive one population while being in the suppressive surround of the other, the anti-phase oscillation is triggered.

(B) Upper: task design; orange and purple dashed circles indicate the RFs of two representative MUA channels. Lower: MUA responses from two example MUA channels from monkey K, each driven either by the disk (orange) or the bar (purple). Inset: theta phases of both channels. Left: the channels' RFs with disk and bar stimuli. Scale bars signify 1°. Shading around lines depicts SEM.

(C) Population distribution of phase differences between disk- and bar-selective channels for both monkeys (monkey K: mean 77° ± 1.6°, n = 385 channel combinations; monkey H: mean 134° ± 5.7°, n = 20 channel combinations).

See also Figure S2.

lesser extent under the single-disk conditions (Figure S1D). To understand better the spatial dependencies of surround suppression on the emergence of theta, we compared MUA responses to a central disk in the RF when two bars where presented either close to (1° away from the disk edge) versus more distant from (2° away) the RF (task timing similar to Figure S2; see STAR Methods). As shown in Figure S1F, more distant surrounding bars resulted in significantly lower theta power than closer surround bars, suggesting that less surround suppression induced by more distant bars results in less MUA theta ($p = 0.007$, $n = 40$ and $p = 7.2 \times 10^{-6}$, $n = 57$ for monkey K and H, respectively; the same trend visible in Figure S1E, lower panels). Finally, MUA power, including the theta band, was much weaker when the suppressing stimulus outside the RF was placed on the opposite hemifield (Figure S1G).

These results therefore extend previous findings of surround suppression effects in V4 [25–28, 34, 35] and demonstrate that placement of multiple objects with respect to neurons' RF center and surround induces theta rhythmic activity.

Theta Emerges from Receptive Field Competition between Neighboring Neuronal Populations

In their recordings from IT neurons, Rollenhagen and Olson [15] observed similar theta oscillations as we did and further demonstrated that the initial phase of the oscillation, whether it was inhibitory or excitatory, depended on the order of the stimulus presentation. We confirmed this result at the level of our V4 MUA assessment by dissociating the onset of center and surround stimulation in time (Figures S2A–S2C): following initial presentation with a stimulus in the RF center, adding flanker stimuli to the surround resulted in a temporary suppression of the response followed by a strong theta rhythmic oscillation. Conversely, when the RF center was stimulated after initial surround stimulation, the theta rhythm started with an initial excitation resulting in an out-of-phase oscillation pattern compared to the previous stimulation condition. Therefore, the location of the second stimulus with respect to the first stimulus and the channel's RF influenced the phase of the resulting oscillation. These phase differences suggest competitive interactions between neighboring neuronal populations. Under our stimulation conditions, one pool of neurons would be excited by the presence of the disk stimulus in their RF, whereas a neighboring pool of neurons would be excited by the presence of one of the flankers in their RF. Disk- and flanker-representing neuronal populations would inhibit each other (Figure 2A). Our recording approach using multi-microelectrode arrays in retinotopically organized V4 allowed us to probe for such RF interactions. To this end, we compared the MUA from electrodes with RFs overlapping either the disk or the flanker stimuli, thereby drawing activity from the two stimulus-representing neuronal populations (Figure 2B). As predicted, the MUA of these electrodes exhibited a simultaneous theta rhythm (Figure 2B; see Figure S2D for a population power-spectrum) but with a prominent phase offset between electrodes with RF coverage of disk versus flanker stimulus (Figure 2C; monkey K: $\Delta\Phi = 77° \pm 1.6°$ [54 ms at 4 Hz], $n = 385$; monkey H: $\Delta\Phi = 134° \pm 5.7°$ [93 ms at 4 Hz], $n = 20$ channel combinations). Estimation of the phase difference based on MUA-MUA cross-correlation lag analysis (see STAR Methods) yielded qualitatively similar results (Figure S2E). This relationship was most stable after onset of the second stimulus and desynchronized slightly over time (Figure S2F).

In other words, high MUA at one electrode site was accompanied by low MUA at the neighboring site, suggesting mutual inhibition mediated by the RF organization as an underlying mechanism of this rhythm (Figure 2A). Further analysis of the different epochs of the trials confirmed the presence of theta-coherent

MUA between electrodes only when both stimuli were present on the screen in both monkeys (Figure S2G). In monkey K with higher signal-to-noise ratios, we also applied MUA-LFP coherence and Granger-causality analysis. The results revealed prominent theta-range MUA-LFP locking (Figure S2H) and a greater Granger-causal influence from bar- to disk-selective MUA channels than the other way around (Figure S2I; the same principle was found as a greater Granger causal influence from disk- to bar-selective channels when stimulus order was reversed). Although differences in MUA power between disk- and bar-responsive channels (Figure S2D) may have biased this effect, the Granger-causality outcome strengthens the interpretation that excitation in MUA channels responsive to the second (bar) stimulus appears to have triggered inhibition in the channels responsive to the first (disk) stimulus (see also Figure 2A).

Microsaccades Cannot Explain the MUA Rhythm

What might be the behavioral correlates of this rhythmic neuronal activity? The results presented so far were all obtained in monkeys maintaining passive fixation within a 1° radius on a central fixation spot while the stimuli were presented in the periphery. The monkeys were not allowed to carry out saccades to the stimuli and eye movements were continuously monitored. However, this leaves the possibility that small fixational eye movements, MSs (Figures 3 and S3A), which could result in brief changes of the visual input to neurons, might have contributed to our effects. MSs have been previously associated with attention [36] and might at least under some conditions even occur rhythmically [1, 18, 37] in tight correspondence with neural rhythms [18, 19, 32, 38]. In our data, MSs, when they occurred, were quite distinct from the observed theta MUA rhythm: MSs were not present in every trial; when MSs occurred during a trial after stimulus onset (63% of trials for monkey K, 48% for monkey H), then not at a fixed latency with respect to stimulus onset and/or with an apparent rhythm (Figures 3A and 3B; note the stimulus-induced suppression of MS occurrence). Across trials, we found MSs to occur about once per s (1.0 ± 0.1 Hz in monkey K and 1.3 ± 0.2 Hz in monkey H), which is a lower frequency compared to the simultaneously measured MUA rhythm (monkey K, 4.1 ± 0.2 Hz; monkey H, 3.4 ± 0.1 Hz) (Figures 3A and 3B). When they were present, MSs triggered a transient MUA response with a peak latency of ~50–200 ms, consistent with previous findings [19, 22, 39], that was arrhythmic (Figures 3C and S3B). We also examined MUA during trials during which no MSs occurred during stimulus presentation. In the example presented in Figure 3D, MSs were only present during the baseline period, yet with no apparent rhythm in the MUA. In contrast, no MSs were present during visual stimulation, yet the center-surround stimulus clearly evoked theta rhythmic MUA modulation. The same pattern was present also when examining the average MUA across all trials without MSs (Figure 3E, upper panel) and when directly comparing theta MUA power in trials with and without MSs across electrodes (Figure 3E), which showed no significant difference ($p = 0.27$, $n = 40$ and $p = 0.83$, $n = 57$ for monkey K and H, respectively). Examination of the MS-LFP relationship gave results that were very similar to the MUA findings (Figures S3C and S3D). In summary, MSs could therefore not account for the stimulus-induced neuronal theta rhythm in our data.

Rhythmic Reaction Time Fluctuations during Distributed Attention

Investigations in humans have demonstrated the presence of rhythmic behavior in the theta range (3–9 Hz) in distributed attention tasks involving multiple objects [7, 11], suggesting that attention might sequentially sample objects over time rather than statically increase the range of its "spotlight." We hypothesized that the theta-modulated MUA evoked by center-surround stimulation in the presence of multiple stimuli (passive viewing) might mechanistically underlie behavioral sampling rhythms present under distributed attention. To test this, we trained the monkeys on a task that employed center-surround stimulation in the context of distributed attention. Monkeys had to detect a small luminance change (target) that was randomly displayed on either the RF center (disk) or the surround stimulus (flanker) by executing a saccade to this location (Figure 4A; see STAR Methods). Similar to the task previously used (Figure S2A) the central disk was presented first, followed by the display of the surround stimulus in addition 500 ms later. Targets were then presented after a randomized period within up to 750 ms following onset of the surround stimulus (flanking bars), allowing the post hoc reconstruction of RTs sorted by target onset times across trials. The monkeys could perform this task with ease (monkey K: 92% correct, 7 sessions, 878 correct trials, mean RTs: disk: 212 ± 6.6 ms, flanker: 220 ± 3.8 ms; monkey H: 96% correct, 8 sessions, 1,509 correct trials, mean RTs: disk: 210 ± 6.9 ms, flanker: 180 ± 6.0 ms). By analyzing the RTs as a function of target onset times, we found that their behavior was not constant across target delays but after an initial masking period (0–250 ms; Figure S4B; see STAR Methods) fluctuated over the assessed time period (250–750 ms). For example, monkey K, at the time point highlighted by the first gray bar in Figure 4B, responded faster to the target when it occurred on the center disk stimulus than when it occurred on the nearby flanker stimulus. Thus, it seems that the monkey's attention was most likely focused on the disk stimulus at this time, requiring reorienting when the target instead occurred on the flanker stimulus. Importantly, this bias toward the disk stimulus was periodic and alternated with periods favoring the competing flanker stimulus, resulting in the overall RT fluctuation over time. We assessed the rhythmicity of these fluctuations by computing their powerspectrum and found a significant peak at 4.3 Hz in monkey K and 5.7 Hz in monkey H for the center stimulus (theta frequency range; Figure 4B, upper right panel; Figure S4A, orange lines; $p = 2 \times 10^{-4}$ and $p = 2 \times 10^{-4}$ for monkey K and $p = 2 \times 10^{-4}$ and $p = 0.01$ for monkey H for the center [orange line] and flanker target [purple line], respectively, randomization test, $n = 5{,}000$). This assessment also confirmed that periods of short RTs for one target location coincided with RT costs for the competing target location (theta phase difference: 95° and 97°, equaling a 66- and 67-ms shift at 4 Hz in monkey K and H, respectively). Control analyses for MS effects also ruled out a contribution under this task condition, with results very similar to the passive viewing condition (Figures S3E–S3G). Thus, monkeys, similar to humans [5, 7, 11], show theta rhythmic RTs under distributed attention and therefore appear to engage in rhythmic attentional sampling under conditions when multiple stimuli compete for perceptual selection.

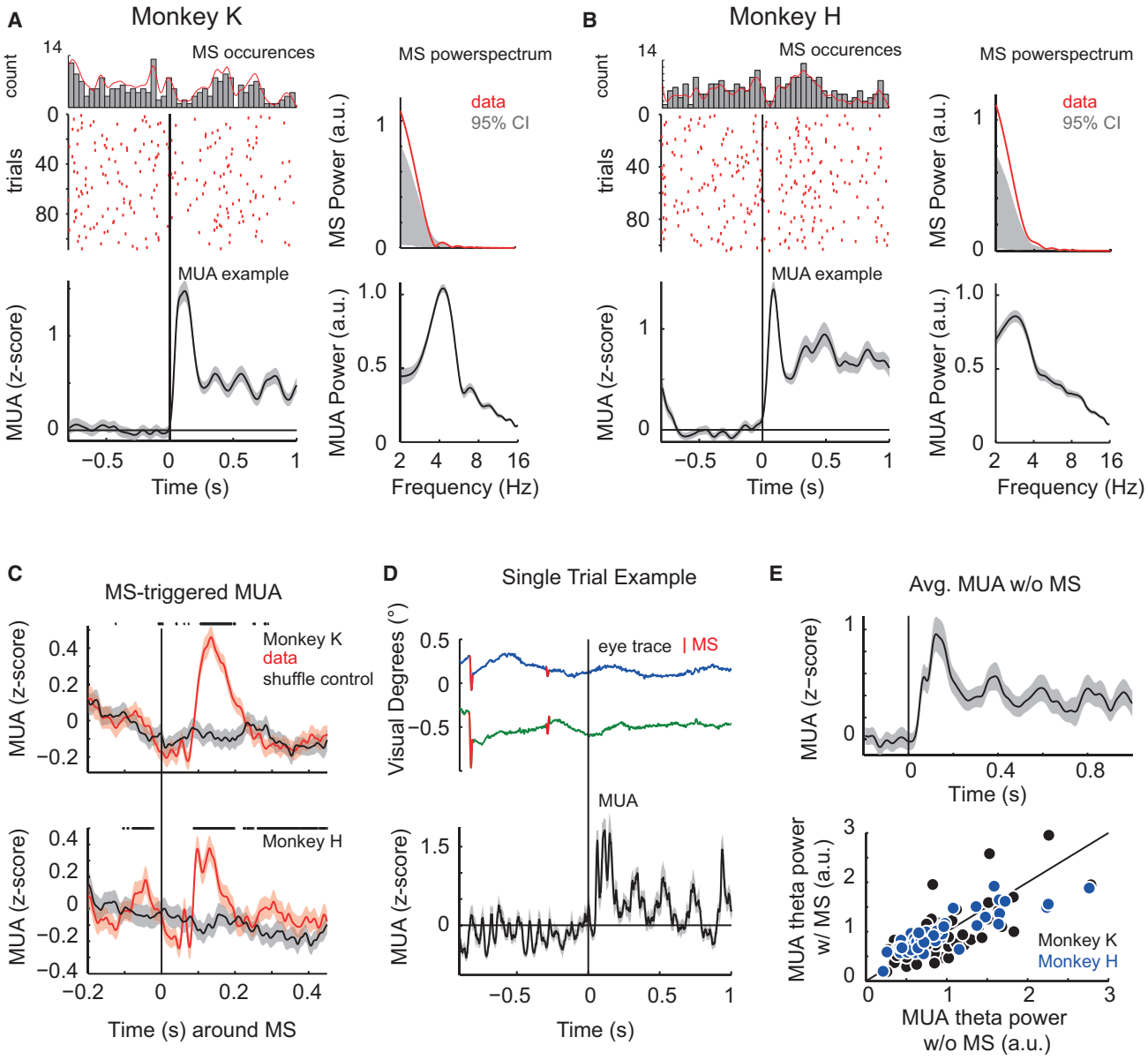

Figure 3. The MUA Rhythm Does Not Depend on Microsaccades

(A) Raster plot shows microsaccade (MS) occurrences over trials and time for passive fixation task (as in Figure 1) of monkey K during presentation of the disk-annulus stimulus. The histogram above shows average MS occurrences across all trials; the red line depicts the smoothed distribution (see STAR Methods). Lower: example MUA response (example channel, averaged across trials). Right: powerspectra of MS occurrences and MUA responses (population average across trials and channels, same as in Figure 1). In 37% (40/108) of the trials, no MS occurred in the time period used for the spectral analysis (0.3–1 s after stimulus onset). CI, confidence interval.

(B) Same as (A), but for monkey H. 52% (54/104) of the trials exhibited no MSs in the spectral analysis window.

(C) MS-triggered MUA from monkey K (upper) and H (lower). Zero represents the time of MS occurrence; the red and gray traces show the actual data and shuffle control, respectively. Stars on top highlight significant differences between both conditions ($p < 0.05$, Bonferroni-Holm corrected for multiple comparisons).

(D) Upper: single-trial example of eye movements of monkey K (x signal, blue; y signal, green). MSs are highlighted in red (n = 2). Lower: a simultaneous single-trial MUA response to a disk-annulus stimulus (disk, 2°; annulus, 6° outer diameter; 4°, inner diameter) averaged across channels (n = 40). The solid vertical line highlights the stimulus onset.

(E) Upper: the average MUA from one example channel from monkey K averaged across trials without MSs after stimulus onset. Lower: comparison of the theta power per channel based on trials with (w/) and without (w/o) MSs for monkey K (black) and H (blue) showing no significant difference ($p = 0.27$, $n = 40$ and $p = 0.83$, $n = 57$ for monkey K and H, respectively, Wilcoxon signed-rank test).

See also Figure S3.

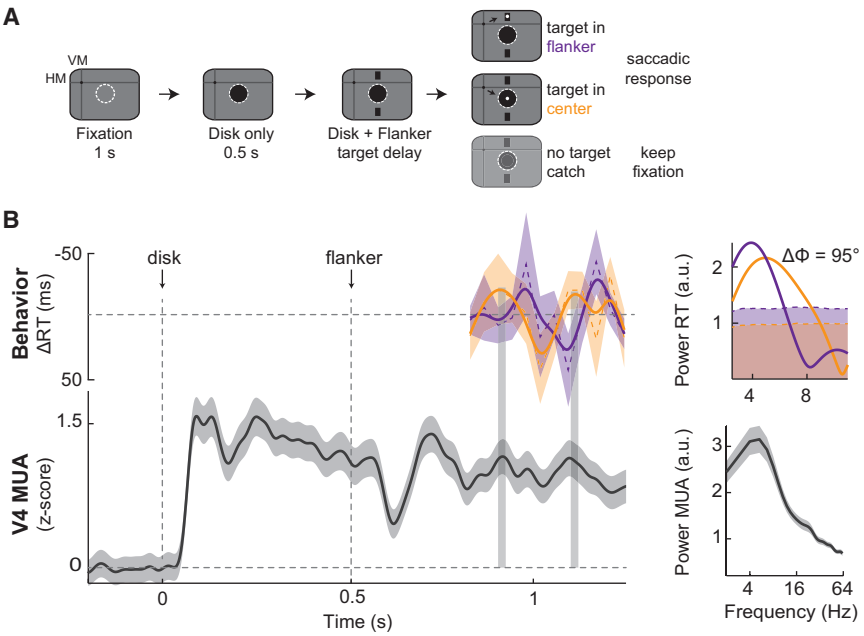

Figure 4. Same Theta Rhythm in MUA and Reaction Times during a Distributed Attention Task

(A) Experimental design. Monkeys had to report a luminance change in either the center (orange) or upper flanker (purple; distributed attention task) by making a saccade toward the respective stimulus change. One-third of the trials were constituted of catch trials where no target appeared.

(B) Upper: the reaction time (RT; normalized as deviation from the mean) from monkey K for distributed attention conditions. RT to the center target position is shown in orange, and to the flanker target position in purple. Non-smoothed RT data are shown as thin dashed lines. Lower: MUA response recorded during catch trials from an example channel (no target appearing; during distributed attention). Vertical gray shaded areas highlight the peak-to-peak locking between the behavioral and neural oscillation (RT to center location [orange] and MUA with corresponding RF). Right: powerspectra of the respective rhythms and the RT phase difference between center and flanker conditions (based on non-smoothed RT data). Shaded areas of RT powerspectra highlight 95% confidence intervals based on shuffled surrogate data (see STAR Methods). Shading around other lines depicts SEM.

See also Figure S4.

Rhythmic Reaction Times Are Coupled to Rhythmic V4 MUA

Analysis of the neuronal data accompanying the behavior during the distributed attention condition revealed the following pattern: after initial excitation through the disk in the RF center, addition of the flankers initiated a suppression in neuronal activity that was reliably followed by a rhythmic oscillation pattern at theta frequencies (Figure 4B, lower panel; also Figures 6A and S5A), similar to the rhythmic fluctuations in RTs. Moreover, when aligning the two signals in time, their relationship became clear (Figure 4B, lower panel): periods of increased MUA during the oscillation were temporally aligned with periods of shorter RTs, whereas lower MUA levels were associated with longer RTs. To quantify this relationship between the RTs and neural oscillations, we computed the cross-correlation between the RT time course across trials to the center target and the MUA recorded during catch trials (Figure 5A). We found significant correlations in 36 of 40 (90%) and 40 of 57 (70%) electrodes ($p < 0.05$, randomization test; see STAR Methods), with mean correlation coefficients of 0.41 ± 0.01 (n = 36) and 0.42 ± 0.01 (n = 40) for monkey K and H, respectively (Figure 5A). Cross-correlations were also prominently rhythmic in the theta range (peak frequencies: 4.6 ± 0.18 Hz, n = 36 and 5.9 ± 0.29 Hz, n = 40; phase shift at peak frequencies: 33.0 ± 7.3 ms and 32.3 ± 11.1 ms; for monkey K and H, respectively), indicating rhythmic synchronization between behavior and neural activity (Figure 5B; significantly theta rhythmic RT-MUA combinations: 36/36 [100%, monkey K] and 40/40 [100%, monkey H], $p < 0.05$, randomization test).

Faster Reaction Times Are Preceded by Larger Responses to the Target Stimulus

So far, the analysis focused on the rhythmic relationship between RT time courses and MUA collected during interspersed catch trials. This was enabled by consistently phase-locked MUA time courses induced by the center-surround stimulus configuration. This analysis revealed the intimate relationship between the behavioral and MUA rhythms across trials. In the next step, we chose a different strategy and instead aimed to directly assess the trial-by-trial representation of the target, i.e., the luminance change, during the course of the observed theta rhythm in the RT. Our rationale was that the representation of the target would be affected by the state, i.e., the phase of the underlying MUA rhythm, and therefore translate into corresponding RTs. More specifically, we reasoned that during the peak periods of the rhythm, neurons might be more sensitive to the target, and therefore respond with greater amplitudes and result in shorter RTs. In other words, if the behavioral modulations were conveyed by rhythmic changes of neuronal excitability, the response of neurons to the physically same target stimulus should differ in strength between fast and slow RTs. To test this for the data collected during the distributed attention task, we quantified the MUA responses to the target stimulus during peak versus trough periods of the RT time course (Figure 6A). Figure 6B shows the average MUA responses to the target across channels (n = 36) recorded during RT peaks and troughs from monkey K. To further quantify this modulation across channels, we normalized these MUA target responses to a MUA baseline that preceded the response by 60 ms, resulting in d prime (d′) as a measure for the neuronal sensitivity to represent the target (see Figure S5B for a sketch illustrating the calculation of d′). Indeed, we found that d′ during peaks of the behavioral oscillation (fast RT period; see STAR Methods for a detailed description) was significantly larger than that during an oscillation trough (Figure 6C; $p = 2.7 \times 10^{-6}$, n = 36 in monkey K; $p = 4.4 \times 10^{-6}$, n = 40 in monkey H; see STAR Methods). Therefore, as predicted, trials with stronger responses

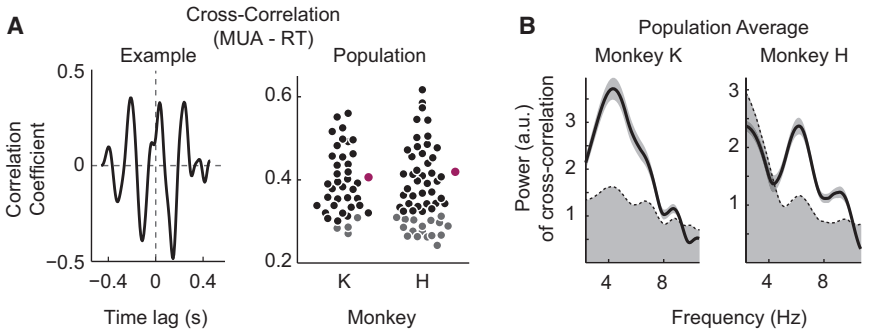

Figure 5. Rhythmic Distributed Attentional Sampling Is Correlated with Cortical MUA Rhythm

(A) Example cross-correlogram between RT and MUA from monkey K during distributed attention (left). Right: the distributions of correlation coefficients of RT-MUA channel combinations for monkey K (left; n = 40) and H (right; n = 57). Electrodes with significant cross-correlations to RT are shown in black (non-significant channels are in gray). The mean MUA-RT cross-correlations across significant electrodes are shown in purple for each monkey.

(B) Powerspectra of cross-correlations for monkey K (left) and H (right) averaged across significantly cross-correlated channels. The shaded area below the dashed line depicts the 95% confidence interval; shading around lines depicts SEM. Note the significant modulation of cross-correlations at theta frequencies.

to the target stimulus resulted in shorter RTs. Additional analysis confirmed, by relating RT to MUA theta phase on a single-trial level, that RTs tended to be shorter, i.e., monkeys were faster around the peak periods of the theta rhythm measured in the MUA (Figure S4C; however, note the drop at 160° in monkey H). Together, these analyses indicate therefore that during the "up states" of the neural theta rhythm, neurons were more sensitive to incoming targets, resulting in shorter RTs during these periods.

DISCUSSION

We found that RF center-surround interactions of V4 neurons induce prominent MUA at theta (~3–6 Hz) frequencies in the presence of multiple visual objects. This theta rhythm was stimulus induced and occurred irrespective of the presence or absence of MSs. When monkeys had to simultaneously monitor the visual objects (distributed attention) to detect an unpredictable luminance change (i.e., the target) in one of the objects, RTs were modulated by a similar theta rhythm as in the MUA. Correlation analyses confirmed a significant locking of RT fluctuations to V4 MUA. Furthermore, the strength of the MUA response to the target change within the theta rhythm was predictive of the monkeys' periodic fast and slow RTs. In the following, we discuss these findings with respect to generative mechanisms of theta oscillations in visual cortex and their function in the context of findings on attentional sampling in humans.

Theta Rhythm in Visual Cortex: Effects of Stimulus Competition and Microsaccades

Assessment of single-unit activity or MUA from visually responsive parts of the brain has resulted in a select number of studies that report theta rhythmic spiking. Neuronal spiking in the theta range has been observed at the cortical level in V4 [14] and IT areas [15, 16, 40, 41] of awake non-human primates. In addition, theta, along with other rhythms, were reported in LFP recordings assessing the role of oscillations for inter-areal communication [18, 42–45]. What are the mechanisms that contribute to the emergence of theta rhythmic activation? In what follows, we discuss how MSs and stimulus competition contributed to the neuronal rhythm in our data and how our findings tie in with the existing literature.

MSs are often observed in the context of attentive, explorative behavior. Recent evidence indicates that at least under some tested conditions, they may occur rhythmically and link to rhythmic neuronal activation (e.g., [18, 19]). In both studies, MSs occurred with a higher likelihood every 250–300 ms, i.e., roughly corresponding to a 3–4 Hz theta rhythm. These theta rhythmic MS occurrences modulated the power of the faster gamma band in the LFP. We therefore tested whether MSs during our paradigm exhibited a similar theta rhythm that could account for the theta rhythmic neuronal modulation in our data. Under our stimulation conditions, MSs occurred at a lower rate than in the Lowet and Bosman studies [18, 19], namely around 1 Hz, consistent with many other reports in the literature [1, 46]. MS rates are influenced by a number of stimulus-related and cognitive factors that most likely explain the variation across studies [46]. For example, MS rate is known to transiently drop after stimulus onset [47] and to increase as a function of fixation duration [1]. In the study of Lowet et al., the time period that was used for the MS analysis was after at least 1.8 s of visual stimulation. Similarly, in the Bosman et al. study, monkeys maintained fixation for several seconds. In our paradigm, under passive fixation, the stimulus duration was 1 s and therefore considerably shorter, which most likely contributed to the lower MS rate in our data. The non-rhythmic average 1 Hz MS rate in our data was lower than the 3-6 Hz rhythm in the MUA and therefore seems to reflect a different process. MSs resulted in transient MUA and LFP responses with peak latencies between 50 and 200 ms, consistent with previous findings in V4 [19, 22]. Additionally, there were no clear differences for the MS-MUA and -LFP relations between passive viewing and distributed attention conditions. Whereas MSs occurred not in every trial and at different times within a trial, theta rhythmic MUA occurred highly consistently across trials, even in the absence of MS. Although our results and similarly the study by Rollenhagen and Olson based on recordings in IT did not show any relationship between the MUA rhythm and MS occurrence during short stimulus presentations, it is conceivable in particular for longer stimulus periods that the stimulus-induced MUA rhythm could trigger the occurrence of rhythmic MSs and overt sampling or that MSs could reset the phase of an ongoing theta rhythm (e.g., [11, 14]).

In our study, theta rhythmic MUA was triggered by the presence of multiple stimuli with respect to the neurons' RFs. This result provides a mechanistic explanation for previous findings

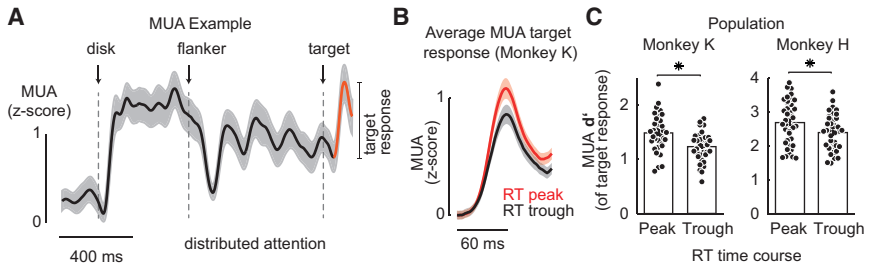

Figure 6. Strength of MUA Response to Target in Relation to Periodic Fast and Slow RTs

(A) MUA from one representative electrode (monkey K) during trials in which the target appeared over the disk stimulus (center position; 1.21 s after stimulus onset). The MUA response to the target's luminance change is highlighted in orange on the background of the stimulus-induced oscillation (black).

(B) Average MUA target response across channels comparing response strength during target delays that corresponded to peaks (red) and troughs (black) of the RT time course (see STAR Methods).

(C) Population distributions of d′ of MUA target responses across channels for RT peaks and troughs for monkey K (left) and H (right) during distributed attention. Asterisks denote significant differences. Shading and error bars depict SEM.

See also Figure S5.

with theta rhythmic activity in visual cortices [14–17, 40, 41] on the basis of center-surround RF interactions (Figures 1 and 2). Increasing the stimulus beyond the RF or adding a second stimulus to the one presented inside the RF both decreased the initial stimulus response as expected from previous results [27] and a sensory normalization mechanism [48]. In line with a reduced suppression drive, the initial stimulus response was intermediate when instead of a single large stimulus only an annulus or bar was shown outside the RF. It is under these intermediate excitation conditions in the presence of two stimuli that MUA became rhythmic (Figures 1 and 2). The oscillation signal was initially negative when the surround (flanker) stimulus was added to the central (RF) stimulus (due to the incoming suppression) and positive under the opposite order, consistent with previous findings [15]. In our V4 array recordings, we could also observe this effect for nearby electrodes likely sampling from neighboring neuron pools (Figure 2), providing evidence for competition-induced theta oscillations in visual cortex occurring at intermediate excitation levels. Under conditions in which the distance between the stimuli was increased, the strength of the rhythm decreased (Figures S1F and S1G), confirming the view that it is a local RF competition that results in the rhythmic MUA modulation. Interestingly, however, the LFP appeared less spatially selective compared to the MUA: although theta modulation in the LFP was strongest during center-surround stimulation, it was also present to a smaller extent during single-stimulus presentations (Figure S1D), possibly representing subthreshold synaptic input from other sources.

Modeling work by Moldakarimov et al. suggested that the emergence of slow oscillatory neuronal spiking activity is influenced by the strength of inhibition between contributing neuronal pools and the timing of spike fatigue and synaptic delay time [30]. Previous experimental research demonstrated that brief (50 ms) presentation of a second stimulus outside the RF in addition to a stimulus inside the RF induces surround suppression in V4 neurons 75–235 ms following stimulus onset, i.e., in the range of a slow theta cycle [27]. Furthermore, increasing the stimulus contrast or directing attention to the surround stimulus was effective in increasing the suppressive effect on the neurons' responses. It appears that our stimulation conditions prolonged this surround suppression mechanism, resulting in theta rhythmic activation. Variability with respect to RF coverage of the stimulus as a function of eccentricity, and consequential latency differences of horizontal connections, is most likely the source for observed frequency and phase variations in our data. Future work will need to clarify how the local connectivity contributes to surround suppression and theta rhythmic spiking, including whether the mechanism is truly inhibitory or better accounted for by a release of excitation. Finally, it will be important to determine whether similar RF competition mechanisms are also underlying the emergence of theta oscillations in other cortical areas with different RF coverage and in the context of other selection tasks, such as during binocular rivalry [16] and working memory [14, 43].

Theta Rhythms during Spatial Attention

We observed theta rhythmic RTs during a distributed attention task that required monkeys to report the occurrence of a spatio-temporally uncertain target. Comparable behavioral results in monkeys were presented by Fiebelkorn et al. (2016, Soc. Neurosci., abstract). In humans, very similar theta rhythmic RT or performance fluctuations have been reported in a number of recent publications in the context of distributed attention [7, 10–12]. It therefore seems likely that the rhythmic RT distributions that we and others observed across paradigms draw upon a more general aspect of theta rhythmic brain function during distributed attention.

An essential aspect employed across investigations on rhythmic performance is to temporally "capture" the locus of attention across trials and subjects by resetting ongoing performance fluctuations to an external event [49, 50]. For example, Landau and Fries reset attentional performance to the onset of a mask stimulus surrounding one of their targets. In our paradigm, the sequential presentation of the two stimuli induced a reset both at the behavioral as well as at the neuronal level. This enabled us to track subsequent rhythmic fluctuations and cross-correlate their time courses in MUAs and RTs. Thus, under the tested conditions, it was an external stimulus event that induced the rhythm. It is therefore conceivable that these visually induced rhythmic fluctuations might reflect bottom-up-driven attentional sampling [11].

The evidence for such a sampling process at the neural level during distributed attention is, however, still very limited at this point. Recently, Jia et al. demonstrated that attention-related EEG alpha oscillations were modulated every 200 ms during distributed attention and that alpha correlated with performance on the unattended object [51]. Furthermore, it has been shown that gamma oscillations in response to a visual stimulus were modulated by theta and that the phase of this theta-gamma coupling was predictive of detection accuracy [12]. Our results

show that a similar theta rhythm is present both at the neural level in MUAs and LFPs as well as in behavioral performance. The presence of two stimuli was associated with a neural theta rhythm where the phase of this neural theta predicted location-specific performance, such as theta "up states," where associated with shorter RTs, and theta "down states," associated with longer RTs. We further showed that these rhythmic states modulated the amplitude of the target-evoked response, so that larger evoked responses resulted in faster RTs. This is consistent with a wide set of findings that the phase of oscillations is predictive of performance and RT fluctuations for near-threshold stimuli ([9, 52–55]; however, see [56, 57]) and reflect fluctuations in neural excitability [50, 58, 59].

At the level of single neurons in V4, a recent study reported reduced responses during uncued (distributed) versus cued (focused) attention conditions [60]. By recording from both hemispheres simultaneously, the authors examined whether they could find any evidence for a switching of responses that may account for attentional sampling of the target locations from both hemifields. The authors did not, however, observe any signs of a switching mechanism in their data. Methodological aspects, such as a short 200-ms analysis window and the absence of a reset event to capture attention, may explain the difference from our results. Moreover, it is possible that no rhythmic activity was observed, as stimuli were spread across hemifields. Our data suggest that local inhibitory input from the same hemifield is a more powerful driver to elicit theta rhythmic activation in V4 compared to an interhemispheric mechanism (Figure S1G).

Our neurophysiological results of theta rhythmic MUA in V4 together with similar observations in higher-order areas [15] provide a direct correlate for theta rhythmic RTs during bottom-up-driven distributed attention. Future research will need to clarify how theta is affected by top-down information, whether there are alternative generative mechanisms for this rhythm, and whether the same mechanism is realized in other areas as well. Here we demonstrate that stimulus-driven center-surround interactions are at the origin of this theta rhythm in V4. Excitation of one population during the theta cycle facilitates transmission of stimulus information from its RF, while at the same time information from the RF location of the neighboring population is suppressed. The duration of a theta cycle (~200 ms) would allow for sufficient time for perceptual processing of at least one object across visual cortical areas [61] in addition to generating a behavioral reaction, such as a saccade to it. The succession of theta cycles as part of the sampling rhythm might act as a dynamic selection mechanism in visual cortex to ensure efficient perceptual processing that may extend also to other parts of the brain in the context of spatial navigation and memory, and therefore constitute a fundamental aspect of brain function.

STAR★METHODS

Detailed methods are provided in the online version of this paper and include the following:

- KEY RESOURCES TABLE
- CONTACT FOR REAGENT AND RESOURCE SHARING
- DATA AND SOFTWARE AVAILABILITY
- EXPERIMENTAL MODEL AND SUBJECT DETAILS
- METHOD DETAILS
- QUANTIFICATION AND STATISTICAL ANALYSIS
  - Spectral Analysis and statistics
  - Analysis of behavioral data
  - MS analysis
  - Neurophysiology and Data Preprocessing
  - Surround Suppression in MUA
  - MUA phase analysis between electrodes
  - RT-MUA relationship on a single trial level
  - Cross-Correlation
  - Strength of MUA response to target for fast versus slow RT periods

SUPPLEMENTAL INFORMATION

Supplemental Information includes five figures and can be found with this article online at https://doi.org/10.1016/j.cub.2018.05.086.

ACKNOWLEDGMENTS

This work was supported by Emmy Noether grant 2806/1 and ERC starting grant 637638 "OptoVision" (to M.C.S.). We thank all ESI staff, the directors Drs. Pascal Fries and Wolf Singer, and in particular Hanka Klon-Lipok, Sabrina Wallrath, Michael Stephan, and Kai Roennburg, and Johannes Boldt and Axel Klug of MPI Tübingen, for their technical support. We are grateful to Drs. Alexander Maier, David A. Leopold, and Alex Thiele for very helpful discussions and comments on a previous manuscript version. The ORCID for R.K. is 0000-0003-2328-3413 and for M.C.S. 0000-0003-1424-130X.

AUTHOR CONTRIBUTIONS

Conceptualization, R.K., J.T.S., and M.C.S.; Methodology, R.K., J.T.S., K.A.S., R.C.S., and M.C.S.; Software, R.K., J.T.S., K.A.S., and K.K.; Formal Analysis, R.K.; Investigation, R.K., K.A.S., and K.K.; Writing – Original Draft, R.K. and M.C.S.; Writing – Review & Editing, R.K., J.T.S., K.A.S., and M.C.S.; Supervision, M.C.S.; Funding Acquisition, M.C.S.

DECLARATION OF INTERESTS

The authors declare no competing interests.

Received: January 22, 2018
Revised: April 26, 2018
Accepted: May 30, 2018
Published: July 12, 2018

REFERENCES

1. Otero-Millan, J., Troncoso, X.G., Macknik, S.L., Serrano-Pedraza, I., and Martinez-Conde, S. (2008). Saccades and microsaccades during visual fixation, exploration, and search: foundations for a common saccadic generator. J. Vis. *8*, 21.
2. Rayner, K. (2009). The 35th Sir Frederick Bartlett Lecture: eye movements and attention in reading, scene perception, and visual search. Q. J. Exp. Psychol. *62*, 1457–1506.
3. Engbert, R., and Mergenthaler, K. (2006). Microsaccades are triggered by low retinal image slip. Proc. Natl. Acad. Sci. USA *103*, 7192–7197.
4. VanRullen, R., Carlson, T., and Cavanagh, P. (2007). The blinking spotlight of attention. Proc. Natl. Acad. Sci. USA *104*, 19204–19209.
5. Dugué, L., Marque, P., and VanRullen, R. (2015). Theta oscillations modulate attentional search performance periodically. J. Cogn. Neurosci. *27*, 945–958.
6. Dugué, L., McLelland, D., Lajous, M., and VanRullen, R. (2015). Attention searches nonuniformly in space and in time. Proc. Natl. Acad. Sci. USA *112*, 15214–15219.

7. Fiebelkorn, I.C., Saalmann, Y.B., and Kastner, S. (2013). Rhythmic sampling within and between objects despite sustained attention at a cued location. Curr. Biol. *23*, 2553–2558.
8. Hanslmayr, S., Volberg, G., Wimber, M., Dalal, S.S., and Greenlee, M.W. (2013). Prestimulus oscillatory phase at 7 Hz gates cortical information flow and visual perception. Curr. Biol. *23*, 2273–2278.
9. Busch, N.A., Dubois, J., and VanRullen, R. (2009). The phase of ongoing EEG oscillations predicts visual perception. J. Neurosci. *29*, 7869–7876.
10. Busch, N.A., and VanRullen, R. (2010). Spontaneous EEG oscillations reveal periodic sampling of visual attention. Proc. Natl. Acad. Sci. USA *107*, 16048–16053.
11. Landau, A.N., and Fries, P. (2012). Attention samples stimuli rhythmically. Curr. Biol. *22*, 1000–1004.
12. Landau, A.N., Schreyer, H.M., van Pelt, S., and Fries, P. (2015). Distributed attention is implemented through theta-rhythmic gamma modulation. Curr. Biol. *25*, 2332–2337.
13. VanRullen, R. (2016). Perceptual cycles. Trends Cogn. Sci. *20*, 723–735.
14. Lee, H., Simpson, G.V., Logothetis, N.K., and Rainer, G. (2005). Phase locking of single neuron activity to theta oscillations during working memory in monkey extrastriate visual cortex. Neuron *45*, 147–156.
15. Rollenhagen, J.E., and Olson, C.R. (2005). Low-frequency oscillations arising from competitive interactions between visual stimuli in macaque inferotemporal cortex. J. Neurophysiol. *94*, 3368–3387.
16. Sheinberg, D.L., and Logothetis, N.K. (1997). The role of temporal cortical areas in perceptual organization. Proc. Natl. Acad. Sci. USA *94*, 3408–3413.
17. Nakamura, K., Mikami, A., and Kubota, K. (1991). Unique oscillatory activity related to visual processing in the temporal pole of monkeys. Neurosci. Res. *12*, 293–299.
18. Lowet, E., Roberts, M.J., Bosman, C.A., Fries, P., and De Weerd, P. (2016). Areas V1 and V2 show microsaccade-related 3–4-Hz covariation in gamma power and frequency. Eur. J. Neurosci. *43*, 1286–1296.
19. Bosman, C.A., Womelsdorf, T., Desimone, R., and Fries, P. (2009). A microsaccadic rhythm modulates gamma-band synchronization and behavior. J. Neurosci. *29*, 9471–9480.
20. De Weerd, P., Peralta, M.R., III, Desimone, R., and Ungerleider, L.G. (1999). Loss of attentional stimulus selection after extrastriate cortical lesions in macaques. Nat. Neurosci. *2*, 753–758.
21. Tolias, A.S., Moore, T., Smirnakis, S.M., Tehovnik, E.J., Siapas, A.G., and Schiller, P.H. (2001). Eye movements modulate visual receptive fields of V4 neurons. Neuron *29*, 757–767.
22. Leopold, D.A., and Logothetis, N.K. (1998). Microsaccades differentially modulate neural activity in the striate and extrastriate visual cortex. Exp. Brain Res. *123*, 341–345.
23. Moran, J., and Desimone, R. (1985). Selective attention gates visual processing in the extrastriate cortex. Science *229*, 782–784.
24. Maunsell, J.H.R. (2015). Neuronal mechanisms of visual attention. Annu. Rev. Vis. Sci. *1*, 373–391.
25. Schein, S.J., and Desimone, R. (1990). Spectral properties of V4 neurons in the macaque. J. Neurosci. *10*, 3369–3389.
26. Desimone, R., and Schein, S.J. (1987). Visual properties of neurons in area V4 of the macaque: sensitivity to stimulus form. J. Neurophysiol. *57*, 835–868.
27. Sundberg, K.A., Mitchell, J.F., and Reynolds, J.H. (2009). Spatial attention modulates center-surround interactions in macaque visual area V4. Neuron *61*, 952–963.
28. Motter, B.C. (1993). Focal attention produces spatially selective processing in visual cortical areas V1, V2, and V4 in the presence of competing stimuli. J. Neurophysiol. *70*, 909–919.
29. Buzsáki, G. (2009). Rhythms of the Brain (Oxford University Press).
30. Moldakarimov, S., Rollenhagen, J.E., Olson, C.R., and Chow, C.C. (2005). Competitive dynamics in cortical responses to visual stimuli. J. Neurophysiol. *94*, 3388–3396.
31. Supèr, H., and Roelfsema, P.R. (2005). Chronic multiunit recordings in behaving animals: advantages and limitations. Prog. Brain Res. *147*, 263–282.
32. Yuval-Greenberg, S., Tomer, O., Keren, A.S., Nelken, I., and Deouell, L.Y. (2008). Transient induced gamma-band response in EEG as a manifestation of miniature saccades. Neuron *58*, 429–441.
33. Cavanaugh, J.R., Bair, W., and Movshon, J.A. (2002). Nature and interaction of signals from the receptive field center and surround in macaque V1 neurons. J. Neurophysiol. *88*, 2530–2546.
34. Pollen, D.A., Przybyszewski, A.W., Rubin, M.A., and Foote, W. (2002). Spatial receptive field organization of macaque V4 neurons. Cereb. Cortex *12*, 601–616.
35. Hegdé, J., and Van Essen, D.C. (2007). A comparative study of shape representation in macaque visual areas V2 and V4. Cereb. Cortex *17*, 1100–1116.
36. Hafed, Z.M., and Clark, J.J. (2002). Microsaccades as an overt measure of covert attention shifts. Vision Res. *42*, 2533–2545.
37. Martinez-Conde, S., Otero-Millan, J., and Macknik, S.L. (2013). The impact of microsaccades on vision: towards a unified theory of saccadic function. Nat. Rev. Neurosci. *14*, 83–96.
38. Amit, R., Abeles, D., Bar-Gad, I., and Yuval-Greenberg, S. (2017). Temporal dynamics of saccades explained by a self-paced process. Sci. Rep. *7*, 886.
39. Martinez-Conde, S., Macknik, S.L., and Hubel, D.H. (2000). Microsaccadic eye movements and firing of single cells in the striate cortex of macaque monkeys. Nat. Neurosci. *3*, 251–258.
40. Tamura, H., and Tanaka, K. (2001). Visual response properties of cells in the ventral and dorsal parts of the macaque inferotemporal cortex. Cereb. Cortex *11*, 384–399.
41. Sato, T., Kawamura, T., and Iwai, E. (1980). Responsiveness of inferotemporal single units to visual pattern stimuli in monkeys performing discrimination. Exp. Brain Res. *38*, 313–319.
42. Bastos, A.M., Vezoli, J., Bosman, C.A., Schoffelen, J.-M., Oostenveld, R., Dowdall, J.R., De Weerd, P., Kennedy, H., and Fries, P. (2015). Visual areas exert feedforward and feedback influences through distinct frequency channels. Neuron *85*, 390–401.
43. Liebe, S., Hoerzer, G.M., Logothetis, N.K., and Rainer, G. (2012). Theta coupling between V4 and prefrontal cortex predicts visual short-term memory performance. Nat. Neurosci. *15*, 456–462, S1–S2.
44. Bosman, C.A., Schoffelen, J.-M., Brunet, N., Oostenveld, R., Bastos, A.M., Womelsdorf, T., Rubehn, B., Stieglitz, T., De Weerd, P., and Fries, P. (2012). Attentional stimulus selection through selective synchronization between monkey visual areas. Neuron *75*, 875–888.
45. Grothe, I., Neitzel, S.D., Mandon, S., and Kreiter, A.K. (2012). Switching neuronal inputs by differential modulations of gamma-band phase-coherence. J. Neurosci. *32*, 16172–16180.
46. Martinez-Conde, S., Macknik, S.L., and Hubel, D.H. (2004). The role of fixational eye movements in visual perception. Nat. Rev. Neurosci. *5*, 229–240.
47. Engbert, R., and Kliegl, R. (2003). Microsaccades uncover the orientation of covert attention. Vision Res. *43*, 1035–1045.
48. Reynolds, J.H., and Heeger, D.J. (2009). The normalization model of attention. Neuron *61*, 168–185.
49. Fiebelkorn, I.C., Foxe, J.J., Butler, J.S., Mercier, M.R., Snyder, A.C., and Molholm, S. (2011). Ready, set, reset: stimulus-locked periodicity in behavioral performance demonstrates the consequences of cross-sensory phase reset. J. Neurosci. *31*, 9971–9981.
50. Schroeder, C.E., and Lakatos, P. (2009). Low-frequency neuronal oscillations as instruments of sensory selection. Trends Neurosci. *32*, 9–18.
51. Jia, J., Liu, L., Fang, F., and Luo, H. (2017). Sequential sampling of visual objects during sustained attention. PLoS Biol. *15*, e2001903.

52. Womelsdorf, T., Fries, P., Mitra, P.P., and Desimone, R. (2006). Gamma-band synchronization in visual cortex predicts speed of change detection. Nature *439*, 733–736.

53. VanRullen, R., Busch, N.A., Drewes, J., and Dubois, J. (2011). Ongoing EEG phase as a trial-by-trial predictor of perceptual and attentional variability. Front. Psychol. *2*, 60.

54. Thut, G., Nietzel, A., Brandt, S.A., and Pascual-Leone, A. (2006). Alpha-band electroencephalographic activity over occipital cortex indexes visuospatial attention bias and predicts visual target detection. J. Neurosci. *26*, 9494–9502.

55. Mathewson, K.E., Gratton, G., Fabiani, M., Beck, D.M., and Ro, T. (2009). To see or not to see: prestimulus alpha phase predicts visual awareness. J. Neurosci. *29*, 2725–2732.

56. Wyart, V., and Tallon-Baudry, C. (2008). Neural dissociation between visual awareness and spatial attention. J. Neurosci. *28*, 2667–2679.

57. Benwell, C.S.Y., Tagliabue, C.F., Veniero, D., Cecere, R., Savazzi, S., and Thut, G. (2017). Prestimulus EEG power predicts conscious awareness but not objective visual performance. eNeuro *4*, ENEURO.0182-17.2017.

58. Dugué, L., Marque, P., and VanRullen, R. (2011). The phase of ongoing oscillations mediates the causal relation between brain excitation and visual perception. J. Neurosci. *31*, 11889–11893.

59. Kundu, B., Johnson, J.S., and Postle, B.R. (2014). Prestimulation phase predicts the TMS-evoked response. J. Neurophysiol. *112*, 1885–1893.

60. Mayo, J.P., and Maunsell, J.H.R. (2016). Graded neuronal modulations related to visual spatial attention. J. Neurosci. *36*, 5353–5361.

61. VanRullen, R., and Thorpe, S.J. (2001). The time course of visual processing: from early perception to decision-making. J. Cogn. Neurosci. *13*, 454–461.

62. Oostenveld, R., Fries, P., Maris, E., and Schoffelen, J.-M. (2011). FieldTrip: open source software for advanced analysis of MEG, EEG, and invasive electrophysiological data. Comput. Intell. Neurosci. *2011*, 156869.

63. Asaad, W.F., and Eskandar, E.N. (2008). A flexible software tool for temporally-precise behavioral control in Matlab. J. Neurosci. Methods *174*, 245–258.

64. Berens, P. (2009). CircStat : a MATLAB toolbox for circular statistics. J. Stat. Softw. *31*, 1–21.

65. Shapcott, K.A., Schmiedt, J.T., Saunders, R.C., Maier, A., Leopold, D.A., and Schmid, M.C. (2016). Correlated activity of cortical neurons survives extensive removal of feedforward sensory input. Sci. Rep. *6*, 34886.

66. Legatt, A.D., Arezzo, J., and Vaughan, H.G., Jr. (1980). Averaged multiple unit activity as an estimate of phasic changes in local neuronal activity: effects of volume-conducted potentials. J. Neurosci. Methods *2*, 203–217.

67. Bair, W., Zohary, E., and Newsome, W.T. (2001). Correlated firing in macaque visual area MT: time scales and relationship to behavior. J. Neurosci. *21*, 1676–1697.

STAR★METHODS

KEY RESOURCES TABLE

REAGENT or RESOURCE	SOURCE	IDENTIFIER
Experimental Models: Organisms/Strains		
Macaca mulatta	Public Health England, Porton Down, UK	Monkey K
		Monkey H
Software and Algorithms		
MATLAB	The MathWorks	https://www.mathworks.com/products/matlab.html
Fieldtrip toolbox	[62]	http://www.fieldtriptoolbox.org/
Other		
Infrared video eye tracking system	EyeLink	https://www.sr-research.com/products/
Data Acquisition Systems	Blackrock Microsystems	http://blackrockmicro.com/neuroscience-research-products/

CONTACT FOR REAGENT AND RESOURCE SHARING

Further information and requests for resources and reagents should be directed to and will be fulfilled by the Lead Contact, Michael C. Schmid (michael.schmid@ncl.ac.uk).

DATA AND SOFTWARE AVAILABILITY

For access to data and software, please contact Michael C Schmid (michael.schmid@ncl.ac.uk).

EXPERIMENTAL MODEL AND SUBJECT DETAILS

Two healthy adult male rhesus monkeys (*Macaca mulatta*, monkey K and H) participated in the study. All procedures were approved by the Regierungspräsidium Darmstadt and carried out in accordance with the applicable laws and regulations according to EU directive 2010/63. The monkeys were group housed in enriched environments of the animal facility and with access to outdoor space. All surgeries were carried out aseptically under general anesthesia using standard techniques including peri-surgical analgesia and monitoring. Each monkey received a titanium-made head-immobilization implant and a recording chamber in addition to Blackrock multi-electrode arrays including a connector implant (Blackrock Microsystems, Hannover, Germany). Throughout the study animal welfare was monitored by veterinarians, technicians and scientists.

METHOD DETAILS

During all the experiments eye movements were tracked using an infrared eye tracking system at a sampling rate of 500 Hz (EyeLink 1000, SR research, Ottawa, ON, Canada). All stimuli were presented on a Samsung 2233RZ LCD screens (120 Hz refresh rate, 1680 × 1050 resolution, viewing distance was 77 cm for monkey K and 86 cm for monkey H). Stimulus presentation and monkey behavior during the experiments were controlled and monitored using MonkeyLogic [63].

For the passive viewing task monkeys were required to keep fixation on a small (0.07° radius) white dot during the entire trial. Usually 1 s of fixation baseline was followed by 1.5 s of stimulus presentation. When two stimuli were presented sequentially, the presentation length of the first stimulus was 0.5 s, while the second was on for 1 s. The intertrial interval was 1 s for all tasks.

For all tasks stimuli were shown in black on a gray (50%) background resulting in 50% contrast. Stimulus luminances were measured after all experiments and were concluded under comparable conditions. The luminance of the gray background was 75 cd/m^2, the luminance of the black disk/annulus/flanker stimuli were 0.9 cd/m^2.

In general, we aimed to use simple stimuli avoiding such with complex characteristics (i.e., gratings) to aid testing center-surround mechanisms without further confounders. As can be seen from Figures 1 and S1, center stimuli resulted in reliable excitation of MUA channels. For the initial RF and suppression testing (Figures 1 and S1) we used black disks with a dimeter of 0.25, 0.5, 1, 2, 3, 4, 6, 7 visual degrees (°). For the disk and annulus task (Figures 1 and S1) annuli of the following sizes were used (inner, outer diameter of annulus): 3°, 6°; 4°, 6°; 3°, 7°; 4°, 7°; 6°, 7°. These annuli were compared to disks with a corresponding diameter (6° or 7°, see Figure S1E, lower panel).

For Figure S1F bars were either 1° or 2° degrees away from the central disk edge and either 1° or 0.5° long (close versus far condition).

For the attention task, monkeys had to fixate a small central white dot within 1° radius (fixation window) during the presentation of the stimuli. After 1 s of fixation baseline a black disk (2° diameter) appeared in the V4 RF. 500 ms later two flanking, vertically orientated bars, each 1° in length and 0.25° in width, appeared on the screen (1° gap between disk and each bar). After flanker onset, a small target (0.2° diameter luminance increase) was flashed on either the central disk or the upper bar (distributed attention) in varying delays. Timing of the target relative to the flanker onset was randomized across trials within a 750 ms time window starting directly after flanker onset (20 × 37.5 ms time points, linearly spaced across the 750 ms resulting in ~26 Hz sampling resolution). I.e., the flanking bars were displayed 500 ms after the onset of the disk – similar to the passive viewing task displayed in Figure S2A – to elicit the consistent theta oscillation. Given the reliable generation of theta rhythm using two flanking bars, we decided to use this stimulus configuration for the attention task as described. The 750 ms period during which the target could appear started immediately after onset of the flanking bars.

In order to receive a liquid juice reward the monkeys had to report their detection of the target by executing a single saccade to the location where the target was flashed within a 1.5° radius window. Monkeys were allowed to execute their saccade up to 500 ms after target presentation. Target contrasts were chosen so that the monkey's mean performance was $\geq$ 90% (contrast as luminance ratio of the target relative to the black stimulus: 0.04 and 0.15 (monkey K), 0.07 and 0.18 (monkey H) for the center and flanker target, respectively). Due to a masking effect arising from the flanker onset and consequential relatively low performance (0.74% and 0.90% in monkey K and H, respectively) we excluded the first 250 ms of the target delay spectrum from further analysis, resulting in a 500 ms RT analysis window.

In addition, catch-trials were randomly included during a third of all trials. Their purpose was to record the stimulus induced oscillations uninterrupted by saccadic responses and to monitor and test monkeys' behavior. During these trials flanker stimuli were presented in addition to the disk stimulus for at least the duration of the longest possible trial in detect conditions without the occurrence of any luminance changes. This ensured that catch trials could not be identified by the monkeys until the end of the trial. In order to receive the reward monkeys had to keep fixation during the entire catch-trial. Otherwise, the timing of stimulus events and the stimulus parameters were identical to the other trials.

QUANTIFICATION AND STATISTICAL ANALYSIS

Spectral Analysis and statistics

To obtain spectral information of MUA and RTs, we performed a spectral analysis using a Hanning-tapered Fourier transformation. Visual inspection of the spectra revealed a prominent peak in the 3-9 Hz, which is referred to as theta throughout the paper. The phase of the oscillation was extracted from the complex Fourier coefficients using the same parameters as above. Spectral peaks were identified as band-limited peaks in powerspectra as judged by visual inspection for each monkey independently. To allow for a more exact peak frequency estimation data was padded (up to 5 s) before calculating the spectral power, which allows for a higher frequency resolution without affecting the actual data.

Time-resolved phase values (Figure S2F) were computed by performing a Fourier-transformation using a hanning-tapered sliding window of 0.5 s length and applying 4 Hz spectral smoothing on a single trial level. Average phases were computed using the "CircStat" MATLAB toolbox for circular statistics [64].

Average values of power within frequency windows were calculated as the mean value across time and frequency.

For all analyses, differences between conditions were tested with nonparametric Wilcoxon signed rank tests (paired data), Mann-Whitney U tests (unpaired data) or computational randomization statistics, if not stated otherwise. Values in the text are always mean ± SEM unless stated otherwise.

To test for significant oscillations, we took the following approach: Since we were interested in neural dynamics that are defined by their specific time-dependent modulations we computed surrogate data that specifically destroyed the timing information of the measured experimental data. The surrogate data was generated by randomly time shuffling the RT courses (detrended, non-smoothed), i.e., randomly re-assigning a given value of the RT vector a new position (index) in the vector. This was repeated 5000 times. In a final step, the very same analysis as for the actual data (spectral analysis, cross-correlation) was performed on the surrogate data (i.e., 5000 time-shuffled trials). From these randomization procedures the p value corresponds to the proportion of times for which the power in the surrogate data exceeded the power in the actual experimental data.

For the quantification of RT course oscillations surrogate data were computed on the non-interpolated RT time courses.

Granger causality, a statistical measure that quantifies to which extent one signal can predict another, was computed in the frequency domain based on fourier coefficients (and the resulting cross-spectral density (CSD) matrix) which were computed using a Hanning-tapered Fourier transformation (as described above) for the different task periods of the passive-viewing disk-bar task (see Figure 2, prestimulus fixation baseline, one-stimulus and two-stimulus period). The computation of granger causality was done using the MATLAB toolbox FieldTrip [62].

Analysis of behavioral data

Behavioral data were processed and analyzed using custom-written code for MATLAB (MathWorks) and the MATLAB toolbox FieldTrip [62]. Only correct trials were used for the analysis. RT was measured as the time between target presentation and the

eye position leaving the fixation radius (1° radius). For the experiments studying the center-surround interactions under passive fixation (Figures 1 and S1) 4 sessions (3358 correct trials in total) in monkey K and 4 sessions (4146 correct trials in total) in monkey H were recorded, i.e., ~105 correct trials per condition (as used in Figures 1 and S1).

For the paradigm with a sequential presentation of disk and bar under passive fixation (Figure 2), 3 sessions (60 correct trials per condition) in monkey K and 2 sessions (30 correct trials per condition) in monkey H were recorded. For the disk flanker timing experiments under passive fixation (Figures S2A–S2C) 2 sessions (41 correct trials per condition) for monkey K and 1 session (20 correct trials per condition) for monkey H were recorded.

With the detection paradigm, we recorded 7 sessions in monkey K (878 correct trials in total, 92% performance (no significant difference between targets), mean RTs: disk: 212 ± 6.6 ms, flanker: 220 ± 3.8ms) and 8 sessions in monkey H (1509 correct trials in total, 96% performance (no significant difference between targets), mean RT disk: 210 ± 6.9 ms, flanker: 180 ± 6.0 ms). Fluctuations of RT time traces ranged from −46 to 42 ms and −14 to 19 ms around the respective mean for monkey K and H, respectively (see Figures 4 and S4).

Due to the relatively high proportion of catch-trials and timing conditions, RT data were pooled across sessions after being normalized session-wise as deviation from mean (resulting in ~20 and ~30 correct trials per target delay for monkey K and H, respectively).

To obtain RT time courses as a function of the variable target onset times across trials (Figures 4 and S4), we calculated the mean and standard error of the mean RT for each target onset time across trials. This results in a vector of mean RTs with an entry for each target onset time. This vector was then detrended using a second order polynomial and smoothed (for display purposes only) using a smoothing spline (MATLAB fit function). Power and phase of the RT time course was then calculated using a Hanning-taped Fourier transformation (on non-smoothed data).

MS analysis

During visual stimulation monkeys were not allowed to perform saccadic eye movements (except for target detection). Nevertheless, during fixation small eye movements (< 1°) can occur. To detect those, we used an algorithm similar to the one introduced by Engbert and Kliegl [47], where MSs are detected as outliers in a velocity-space. Detection threshold were set to 5 standard deviations of the velocity distribution. In order to perform a spectral analysis of MS occurrences MS-time points detected in the same time window used for the MUA spectral analysis (0.3-1 s after stimulus onset) were pooled across trials and used to compute a probability density estimate based on a normal (kernel) function (bandwidth = 0.18). This was then used to compute the powerspectra in the same way as for the MUA.

The reported MS-rate of ~1 Hz was assessed by relating the number of occurred MS in the respective analysis window to its length, resulting in an average MS-rate across trials (e.g., 1 MS in the 0.75 ms window in trial 1, 0 MS in the 0.75 ms window in trial 2, 2 MS in the 0.75 ms window in trial 3, etc.).

To compute MS-triggered MUA and LFP the time-stamps of MS were extracted and then used as a trigger to align MUA and LFP across trials per channel (recorded during the Figure 1 passive viewing task with the disk-annulus stimulus that elicited rhythmic MUA and the attention task). The shuffle control data (Figures 3C, S3D, S3F, and S3G, gray lines) was computed by performing the same analysis but using MS timings and MUA (and LFP) from separate trials. The power of MS-triggered MUA and LFP was calculated in the time-period following the MS. p values in Figure 3C were computed across trials using the trial-averaged MUA and corrected for multiple comparisons using the Bonferroni-Holm correction.

Neurophysiology and Data Preprocessing

Neurophysiological data was recorded from 64 channel Blackrock multi-microelectrode "Utah" arrays (Blackrock Microsystems, Hannover, Germany) that were chronically implanted in the left hemisphere's area V4 (prelunate gyrus). Electrodes had lengths of either 0.6 or 1 mm arranged in alternating sets of two rows of short and long electrodes. Each electrode was 400 μm away from its neighboring electrodes. Reference wires were inserted over parietal cortex and cerebellum. Neural data was recorded at a sampling rate of 30 kHz using a Blackrock Microsystems Cerebus system.

All neurophysiological data were processed and analyzed using custom-written code for MATLAB (MathWorks) and the MATLAB toolbox FieldTrip [62]. The continuous recordings were separated into trials using digital event markers and aligned on stimulus onset. We focused our analyses on the sustained periods excluding the transient onset response (300 - 1000 ms after stimulus onset).

An estimate for MUA was obtained from the high frequency envelope: MUA was extracted from the raw data by high-pass filtering (300 Hz), rectification, low-pass filtering (120 Hz) and then downsampling to 500 Hz [31, 65, 66]. Data from microelectrode arrays were z-scored per session and then pooled across sessions considering the data as dependent across sessions.

In order to assess the stimulus-specific effects of neuronal spiking MUA data were z-scored channel-wise based on the average prestimulus fixation period (700 ms before stimulus onset). MUA is therefore expressed as z-score values throughout the paper.

RFs were mapped for each electrode channel by quantifying their responses to small gratings with a Gaussian mask (0.375° SD, cut off at 6 SD from center, 100% contrast, moving upward or downward with 1.5 cycles/s, spatial frequency 1.5 cycles/°) presented at 63 positions for monkey K (34 for monkey H) in the lower right quadrant in the range x = 1 to 5.5° and y = −4 to 2° for monkey K (x = 0.5 to 3.5° and y = −5 to −0.5° for monkey H). The resulting response matrix was convolved with a Gaussian window for display purposes only. The RF focus was defined as the position eliciting the maximal response. To be included into further analyses the Euclidian distance between a channel's RF focus and the stimulus center had to be less than 1.5° (40 and 57 channels in monkey K and H, respectively). This ensured that stimuli were presented into channels' excitatory center.

Mean RF centers were located at 2.9° ± 0.1° (std = 1.17°) (x axis) and −0.8° ± 0.1° (std = 1.4°) (y axis) and 1.4° ± 0.1° (std = 0.53°) (x axis) and −1.8° ± 0.1° (std = 0.9°) (y axis) in monkey K and H, respectively.

Surround Suppression in MUA

We defined the RF center as the diameter of the stimulus that elicited the strongest average activation (across trials and post-stimulus time) in a given channel. To quantify the maximal suppression induced by stimulating the RF inhibitory surround, we identified the stimulus with a larger diameter than the RF center that elicited the minimal average activation within the tested stimulus sizes and computed their relationship as follows:

$$SI = \frac{A_{max} - A_{min}}{A_{max}} \quad \text{(Equation 1)}$$

where SI is the Suppression Index, A_{max} is the maximal and A_{min} the minimal MUA.

The maximal response had to be significantly larger than baseline activity (40/41 channels in monkey K, 57/57 channels in monkey H). By visual inspection, 15% (n = 6/40) and 33% (n = 19/57) channels showed asymptotic suppression in monkey K and H, respectively (Figure S1). The mean size of the center summation RF across channels was 1.7° ± 0.2° (n = 40) and 0.9° ± 0.1° (n = 57) in monkey K and H, respectively.

To quantify the change in theta power as a function of suppression increase (Figure S1), we computed a theta index either between theta power in response to a 2° disk versus larger disks (3°,4°,6°,7°) or of larger disks (3°,4°, 6° 7°) and disk-annulus stimuli with a 2° central disk and varying annulus sizes (6°,3°; 6°,4°; 7°,3°; 7°,4°; 7°,6°; outer and inner annulus diameter respectively). For the latter comparison the outer diameter of the annulus always matched the large disks in size to ensure that both stimuli reached into the surround by the same distance. The theta index was computed as follows:

$$TI = \frac{(ls - ss)}{(ls + ss)} \quad \text{(Equation 2)}$$

where *ls* and *ss* are the theta powers in response to a large and small stimulus, respectively. In case of the disk versus disk-annulus comparison, *ls* and *ss* are the theta powers in response to a disk-annulus and corresponding large disk stimulus, respectively.

MUA phase analysis between electrodes

For the phase analysis displayed in Figures 2B and 2C electrode channels were selected and grouped depending on whether MUA response was stronger for the disk or the flanker stimulus position. In addition, theta power in the post-stimulus period excluding the transient had to be significantly larger than that during the fixation baseline and contain significant theta oscillatory power. This ensured that we performed the phase analysis only on channels that showed significant theta oscillations and were (relatively) selective to one of the two stimulus positions. Note that this selection of channels with significant theta oscillations was only performed in this particular analysis. In all other analyses channels were selected independently of theta power.

RT-MUA relationship on a single trial level

Assessment of MUA theta phases (Figure S4B) was done by calculating the fourier coefficients of the MUA recorded during detection trials of the attention task (0.5 s after disk onset until end of target response) using a hanning-tapered sliding window of 0.5 s length and applying 4 Hz spectral smoothing on a single trial level. Phases were then extracted at the time point of target presentation, i.e., not at the time of the target signal arriving at V4, due to short trial length. To estimate the phase at which the target signal arrives in V4, ∼100 ms (conduction delay to V4), equaling a phase difference of 144° at 4 Hz, have to be added to the resulting phase.

RTs were normalized (divided by average) per session.

Cross-Correlation

In order to quantify the relationship between the theta modulation in behavior and MUA, we computed cross-correlations between the mean RT time-trace and the MUA signal of each channel for both monkeys as follows [67]:

$$CC_{n_1,n_2}(\tau) = \sum_{t=1}^{T} (P_{RT}(t) P_{\mathrm{MUA}}(t+\tau) \quad \text{(Equation 3)}$$

where T is the number of discrete time bins, t is time, P_{RT} and P_{MUA} are the normalized RTs and MUA PSTHs (averaged across trials, mean subtracted), τ is time lag and CC_{n_1,n_2} is the cross-correlation. Before computing the cross-correlation we inverted the RTs (as seen in Figure 4B) such that a positive cross-correlation signifies a coincidence of a high MUA response and fast RTs.

Before performing the cross-correlation both the RT (detrended, but non-smoothed) and MUA signals were resampled to 150 Hz (requiring "interpolation" of RT) to ensure that similar time points of both signals are used for the computation. We used time lags between -450 ms and +450 ms. Cross-correlograms were then normalized such that the correlation coefficient of the autocorrelation at zero lag equals 1.

Correlation coefficients were extracted from the cross-correlations by identifying the maximum value within ± 125 ms around 0. To test for a possible rhythmic modulation we computed powerspectra of the cross-correlations (see Spectral Analysis and Statistics for further information) based on the actual data and on those computed from the surrogate data (see above).

For the cross-correlation lag analysis (Figure S2E) the cross-correlation was computed in a similar way but between MUA channels from the two different neuronal groups (disk- and bar-selective, selection criteria as described above, see also Figure 2), i.e., P_{RT} and P_{MUA} both are normalized MUA PSTHs on a single trial level. The lag was defined as the latency from the peak of the cross-correlogram occurring ± 125 ms around 0. Times were converted into degrees assuming a 4 Hz oscillation.

Strength of MUA response to target for fast versus slow RT periods

To quantify the strength of the MUA response to the target (luminance change) with respect to baseline we computed the d' as a measure of sensitivity as follows:

$$d' = \frac{\mu_p - \mu_b}{\sqrt{\frac{1}{2}\left(\sigma_p^2 + \sigma_b^2\right)}} \quad \text{(Equation 4)}$$

where $\boldsymbol{\mu_p}$ and $\boldsymbol{\mu_b}$ are the means and $\boldsymbol{\sigma_p}$, $\boldsymbol{\sigma_b}$ the standard deviations for the MUA of the peak and the baseline preceding the peak by 60ms, respectively. This analysis was performed on MUA recorded during detection trials (distributed attention condition) during target delay conditions associated with a peak in the RT course (i.e., fast RT; 0.9 and 1.1 s for monkey K and 0.85 and 1.02 s for monkey H) versus target delay conditions associated with a trough (slow RT; 0.82 and 1.01 s for monkey K and 0.78 and 0.98 s for monkey H). Peaks were detected for each condition and channel separately.

Current Biology, Volume *28*

Supplemental Information

Theta Rhythmic Neuronal Activity and Reaction Times Arising from Cortical Receptive Field Interactions during Distributed Attention

Ricardo Kienitz, Joscha T. Schmiedt, Katharine A. Shapcott, Kleopatra Kouroupaki, Richard C. Saunders, and Michael Christoph Schmid

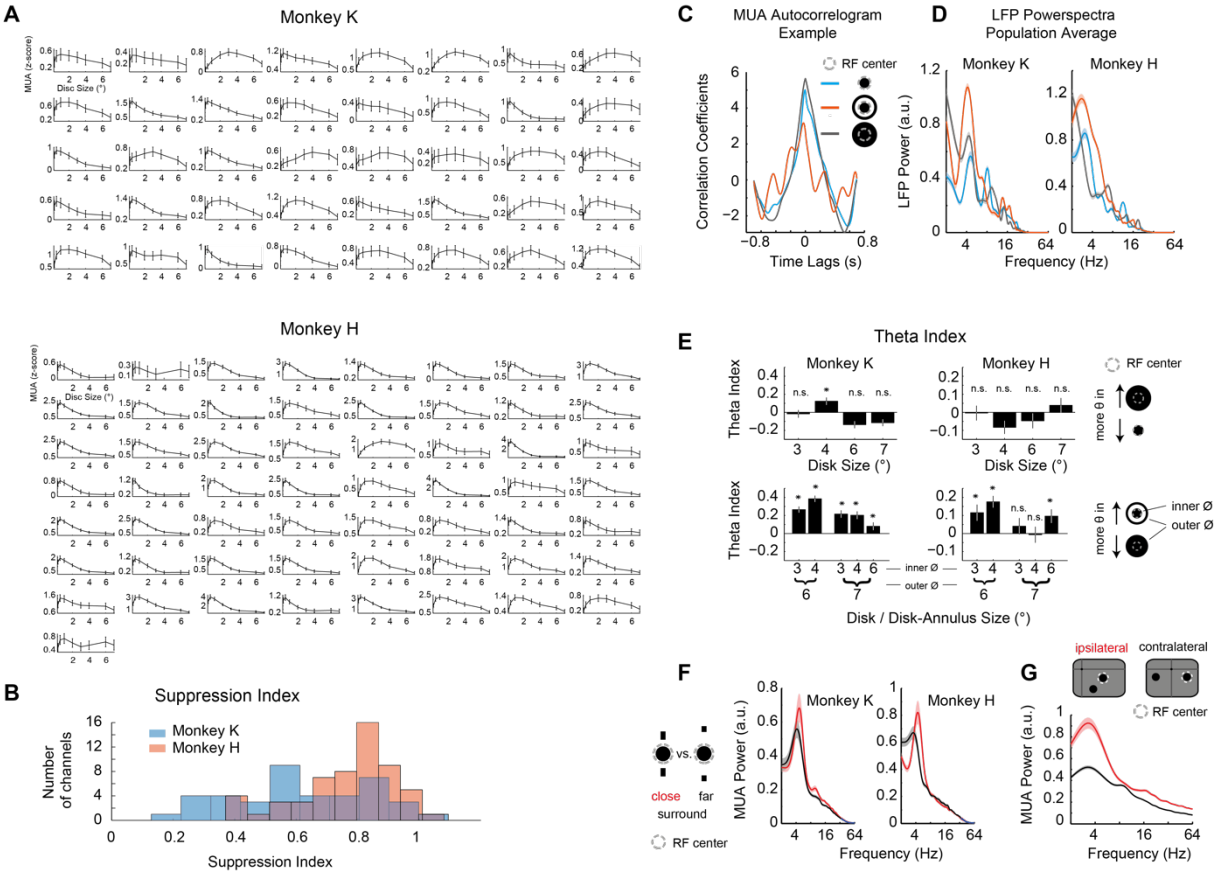

Figure S1. Surround suppression and theta oscillations, Related to Figure 1.

(A) Size tuning curves of all included channels (average across trials) from monkey K (top panel) and monkey H (lower panel).

(B) Distribution of SI values from monkey K (blue, mean = 0.62 ± 0.03, n = 40) and monkey H (red, mean = 0.77 ± 0.02, n = 57).

(C) Example MUA autocorrelogram from the same channel as in **Figure 1B-C** with the same color conventions (small 2° disk (blue); large 6° disk (gray); 2° disk with 4-6° annulus (orange), see also little insets). Note the oscillation in the disk-annulus condition only (orange) that resembles the findings of the spectral analysis in **Figure 1B.**

(D) Population average of LFP powerspectra across channels for monkey K (left panel) and H (right panel), same color convention as in (C) and in **Figure 1B-C**. Note the presence of a peak in the theta range and that strongest theta power is found in the disk-annulus condition (orange).

(E) Upper Row: Distributions of theta indices comparing the theta power of a 2° disk (diameter), roughly corresponding to the RF center, vs. lager disks also stimulating the RF surround (3°, 4°, 6°, 7° in diameter). Positive values indicate higher theta power for the larger disk (presence of inhibition). Note that no theta peak was visible in the powerspectra for both small and large disks (**Figure 1**) indicating that higher power values represent unspecific over-all power shifts.

Lower Row: Distributions of theta indices comparing the theta power of large disks and disk-annulus stimuli with the same outer diameter, i.e. same spatial extent into

suppressive surround. Positive values indicate higher theta power for the disk-annulus stimuli.

(F) Powerspectra show MUA power averaged across channels during the passive viewing disk-flanker task (see **Figure S2**) comparing conditions where the bars falling in the suppressive surround are close to the central disk (red lines, 1° gap, 1° bar length) and further away (black lines, 2° gap, 0.5° bar length) from monkey K (left) and H (right), showing lower theta power when suppression is reduced.

(G) Powerspectrum showing MUA power averaged across channels from monkey K recorded during a passive viewing task (1s fixation, 1s stimulus presentation) comparing two conditions where two disks (black, 2° diameter) are either displayed in one hemifield (red lines, *ipsilateral*) vs. both hemifields (black lines, *contralateral*).

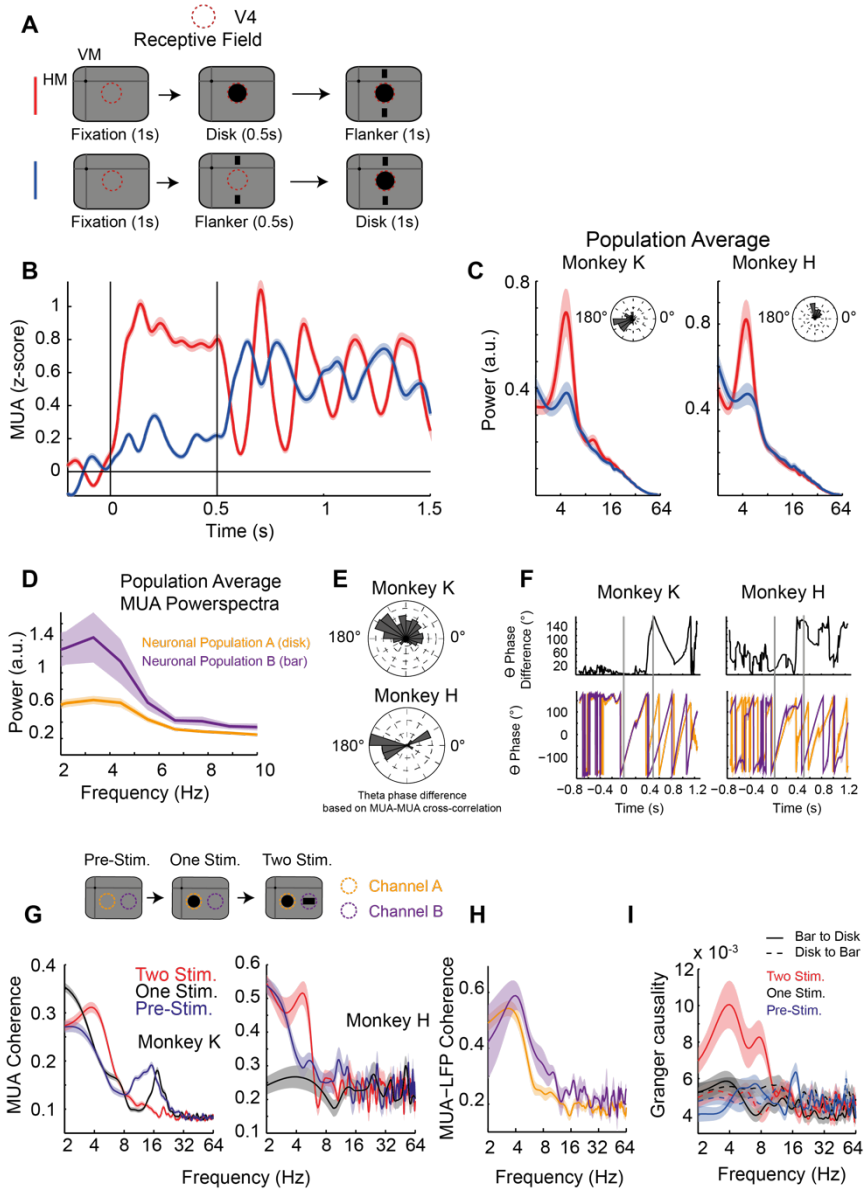

Figure S2. Stimulus timing and location controls phase, Related to Figure 2.

(A) Experimental design involving passive viewing disk-flanker stimulation providing the data shown in **B-C**. After 1s of fixation either the disk (in RF center, red) or the flanker (in RF suppressive surround, blue) appeared first, followed by the respective other stimulus.

(B) MUA responses from one example channel of monkey K to the two different stimulation conditions (averaged across trials), same color conventions as in (A).

(C) Population powerspectra of monkey K (left panel) and monkey H (right panel) with phase plots showing the channel-wise theta phase-differences between the two conditions of monkey K (left panel) and monkey H (right panel) across channels (mean: -168.6° ± 6.7°, n = 40 for monkey K; mean: 93.8° ± 7.3°, n = 57), same color conventions as in (A).

(D) Population average powerspectra across MUA channels of monkey K of the task involving the sequential presentation of disk and bar as displayed in **Figure 2**.

(E) Rose plots showing the distribution of phase differences between the two adjacent

neuronal populations as displayed in **Figure 2** from monkey K (left) and H (right) based on cross-correlation lag-analysis (see Methods).

(F) Lower panels depict phase plots showing the MUA theta phase across time recorded during the disk-bar task (**Figure 2**) from monkey K (left panel) and monkey H (right panel). Upper panels depict the corresponding phase difference between both neuronal groups (0°: in phase, 180°: out-of-phase). Vertical lines highlight stimulus onsets. Same color conventions as in Figure 2 and S2D.

(G) Spectra depict MUA-MUA coherence between the two neighboring neuronal populations as displayed in **Figure 2** from monkey K (left) and H (right) averaged across MUA channel combinations for the prestimulus fixation period (blue lines), the one-stimulus only period (black lines) and the two-stimulus period (red lines). Note that theta coherence is only present when the neighboring stimuli are displayed (red liens).

(H) Spectrum depicts the MUA-LFP coherence from monkey K during the two-stimulus period of the disk-bar task (**Figure 2, S2G**). Same color conventions as in **Figure 2, S2D.**

(I) Granger causality spectrum from monkey K for the same conditions as in (**G**). Solid lines depict granger causal influences from the bar-selective to the disk-selective MUA channels (dashed line vice versa). Note that granger causal interactions are present only during the two-stimulus period and are directed from bar- to disk-selective MUA channels.

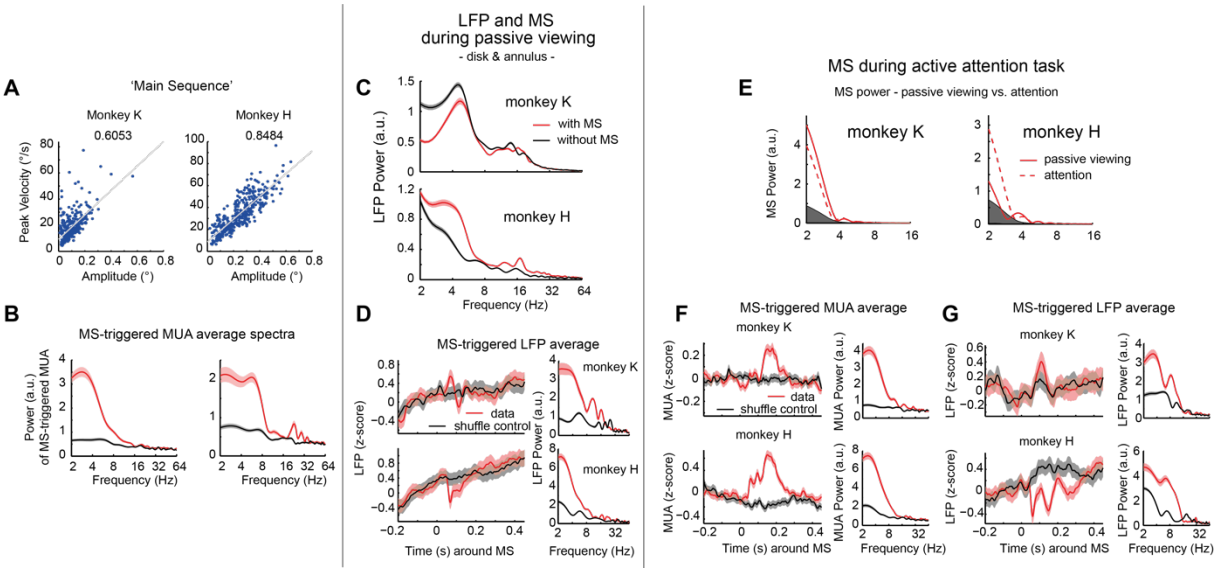

Figure S3. Microsaccade (MS) main sequence and MS analysis, Related to Figure 3.

(A) Main sequence of microsaccades (MS) for monkey K (left) and H (right) showing the relation of amplitude and peak velocity of each MS and the respective correlation values across MS.

(B) Average Powerspectra of MS-triggered MUA computed during the same task as in **Figures 1, 3** after MS onset for monkey K (left) and H (right) showing the actual data (red) and trial-shuffled control data (gray).

(C) Average LFP powerspectra from monkey K (upper panel) and H (lower panel) based on trials with (red lines) and without MS (black lines) recorded during the disk-annulus passive viewing task (as also displayed in **Figures 1, 3**).

(D) Left panels show MS-triggered LFP average (actual data: red lines, shuffle control: black lines), right panels depict powerspectra of the MS-triggered LFP average. Upper rows show data from monkey K, lower panels from monkey H.

(E) Powerspectra of MS during the disk-annulus passive viewing task (solid red lines) and the attention task (dashed red lines) from monkey K (left) and H (right). Shaded area depicts 95% confidence interval based on shuffle controls.

(F) Same as (D), but for MS-triggered MUA average recorded during the attention task.

(G) Same as (D), (F), but for MS-triggered LFP average recorded during the attention task. Shaded areas depict SEM, if not stated otherwise.

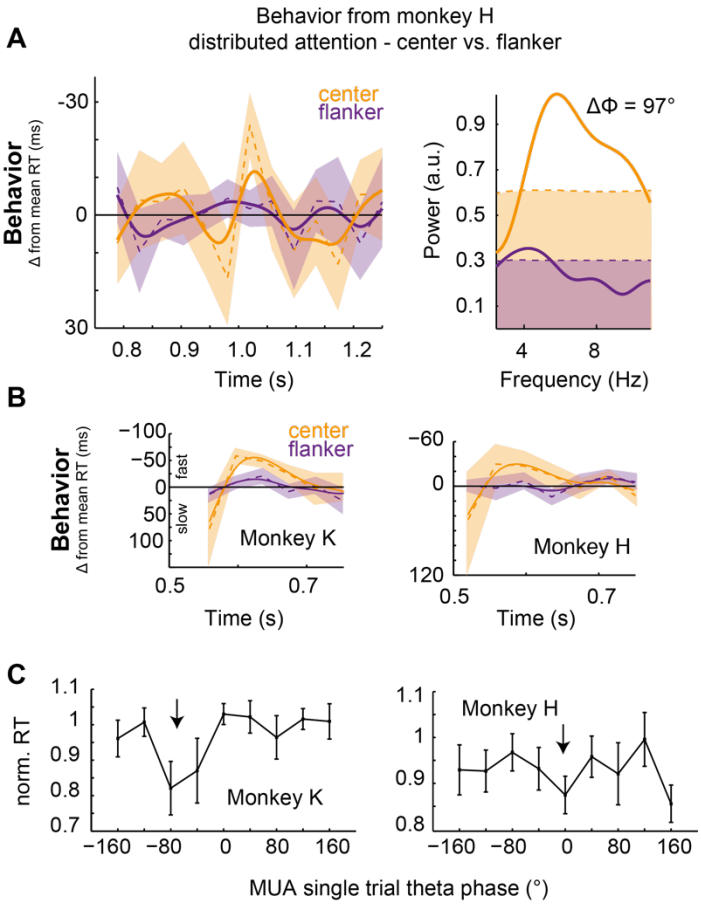

Figure S4. Reaction time data of Monkey H, Related to Figure 4.

(A) Left panel showing the reaction time (as deviation from mean) as a function of target delay for the distributed attention condition in response to the center (solid line) and flanker target position (dashed line). Non-smoothed RT data shown as thin dashed lines, shadings around lines depict SEM. Right panel depicts powerspectra of the respective non-smoothed RT data and their phase difference (97°). Shadings represent 95% confidence intervals based on shuffled surrogate data.

(B) Left panel shows RT data including the part excluded elsewhere due to a masking effect from monkey K (first data point not discernible due to 0% performance). Right panel shows same data from monkey H. Same color convention as in (A).

(C) Average normalized reaction times are plotted against MUA theta phase (0° corresponding to the oscillation's peak) on a single trial level estimated at target presentation time from monkey K (left) and H (right). Error bars indicate SEM, arrows indicate MUA theta phase of fast RT.

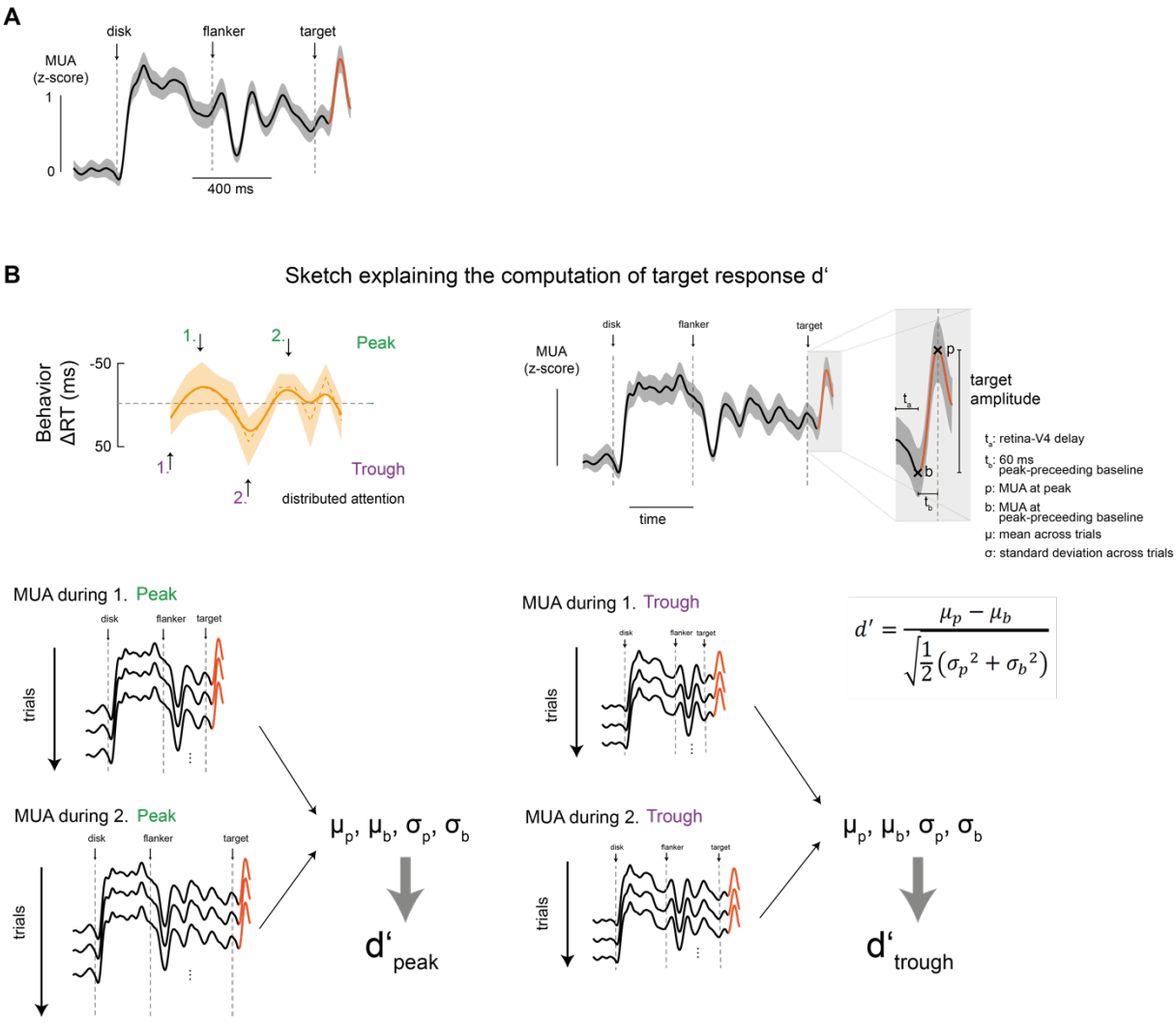

Figure S5. MUA target response and the computation of d', Related to Figure 6.

(A) Example MUA channel, averaged across trials, recorded during the distributed attention task where the target presentation falls onto a trough / rising part of the ongoing oscillation. Compare to **Figure 6A**.

(B) Sketch illustrating the computation of the d' quantifying the target response. Upper left panel shows the RT trace of monkey K highlighting the peaks and troughs and the corresponding SOA conditions that were used to analyze MUA and its target responses during the distributed attention task. Upper right panel explains how the quantification of target responses and d' was calculated. The peak amplitude was defined as the amplitude difference between the peak and the baseline that preceded the peak by 60 ms. It was then related to its variation across trials as shown in the d' equation. The lower panels illustrate that the target responses were quantified across trials for the selected RT peak and trough SOAs.